DOE/ER/3072-38
September 2, 1986
DRAFT

PROPOSAL FOR EXPERIMENTAL STUDIES OF NONLINEAR QUANTUM ELECTRODYNAMICS

K.T. McDONALD
Princeton University

Table of Contents

1. Overview of the Proposed Experiments in Nonlinear Quantum Electrodynamics.

We propose to undertake a series of experiments to study the behavior of free electrons and photons in very strong electromagnetic fields of macroscopic extent. The recent development of intense 'table-top' lasers permits short pulses of light to achieve fields strengths of $\sim 10^{11}$ V/cm over a focal spot of a few optical wavelengths, for a relatively modest cost. In the rest frame of a 50-GeV electron, the field strength is then $\sim 10^{16}$ V/cm. This is similar to the QED critical field strength

$$E_{\rm crit} = m^2c^3/e\hbar = 1.32 \times 10^{16} \text{ V/cm} \quad (= 4.41 \times 10^{13} \text{ gauss}),$$

for which the voltage drop across a Compton wavelength is the electron rest energy. Fields of this strength are unstable against breakdown via electron-positron pair production, and will manifest various other nonlinear aspects we wish to study.

The experiments all are based on bringing a high-energy electron or photon beam into collision with a high-intensity laser beam. The present proposal is for a demonstration experiment with a 25-MeV electron beam and a moderately intense laser. This experiment is introduced in section 1-1. The next set of experiments will use a 50-GeV electron beam and an upgraded laser system to study various effects including true light-by-light scattering, as mentioned in sections 1-2. In section 1-3 we speculate as to how the program could evolve to explore novel nonlinear processes as the technology of high-intensity lasers improves. Section 2 then reviews the understanding of these nonlinear effects in the absence of any experimental studies. Details of the 25-MeV experiment are presented in section 3, followed by a discussion of the laser system in section 4. Some features of the proposed experimental program have been published elsewhere.[1]

Nonlinear QED effects can also be explored, for example, by probing the electric field of a heavy nucleus, with interesting and controversial results.[2,3] In the present approach the strong electromagnetic field is a collection of photons in nearly the same state–a laser beam, and the probe is a single electron, or photon. Although the center-of-mass energies will be low, the spirit of investigation is that of high-energy physics. That is, we seek to extend our laboratory knowledge of fundamental processes by examining relatively simple situations compatible with detailed theoretical interpretation.

1-1. Nonlinear Thomson Scattering.

The first experiment is designed to demonstrate that an ultrashort laser pulse can be brought into collision with a single rf bunch of a linear electron accelerator, while also investigating the simplest nonlinear effect of a free electron in a strong electromagnetic field. This latter effect is a correction to Thomson scattering in which several photons may be absorbed by the electron before a single (higher energy) photon is radiated. This only becomes probable when the electron is placed in a field so strong that sizable 'transverse mass' corrections apply, which affect the kinematics of the scattering in a noticeable manner. As discussed in section 2 below, these effects have a semiclassical origin, and are not dependent on vacuum polarization.

The experiment will be conducted at the Accelerator Test Facility[4] which is to be built at Brookhaven Lab. This is a 50-MeV electron linac with extremely small emittance ($\sim 1.5 \times 10^{-10}$ m-rad when driven by a photocathode gun). We plan to operate the linac at 25 Mev for reasons discussed in section 3. A Nd:glass laser, operating at 1.05-μm wavelength, will produce pulses 1-2 ps wide of energy 100 mJoule at a repetition rate of a few Hertz. Part of each pulse will be used to trigger the photocathode gun of the linac so as to maintain precise synchronization between the laser and the linac. The main laser pulse will be brought into head-on collision with the linac beam. Photons which backscatter out of the laser beam will be Doppler-shifted to about 10 keV, where they can be well analyzed in an x-ray spectrometer. As this experiment will require close interaction between the laser and the linac, the author is also a member of the collaboration to construct the Accelerator Test Facility.

As a technical byproduct, we note that the x-ray beam resulting from this experiment will have a peak brightness greater than that recently obtained at the Novette facilty of LLNL,[5] and comparable to that of the proposed Advanced Photon Research Facility[6] (a synchrotron light source). Although the duty factor will be low, this x-ray capability may be of some interest to the materials physics community.

An exciting aspect of the Accelerator Test Facility is the experiment to demonstrate the laser-driven grating accelerator.[7] For this a CO_2 laser, with 10-μm wavelength, is being constructed. The maximum energy gradient achievable with this approach will be limited by the onset of surface damage (*i.e.*, plasma formation) induced by the laser. The 1-μm laser of the present proposal may well lead to a

different damage limit than that for the CO_2 laser. In addition, it is relatively straightforward to produce laser beams of the 2^{nd}, 3^{rd}, and 4^{th} harmonics of the Nd:glass laser using techniques of nonlinear optics, while no such harmonic generation is feasible for the CO_2 laser. Hence the grating accelerator could be explored at four additional frequencies using the present laser, which may prove more favorable because of materials limitations, despite the greater difficulty of making the grating structures at shorter wavelengths.

1-2. Second Round Experiments.

Following the success of the first experiment, an upgraded version of the laser could be transferred to the C line at SLAC, which has been the scene of past laser backscattering experiments. The program would greatly benefit if the C line could be upgraded to transport the 50-GeV beam which will available as a result of the SLC project.

The second experiment is essentially the same as the first, but now conducted with 30–50-GeV electrons. In this case Thomson scattering is better descibed via quantum mechanics as Compton scattering, as the multiphoton effects mentioned above are now also subject to quantum corrections.

For the third and fourth experiments, a beam of backscattered photons is brought into collision with a laser beam, resulting in a light-by-light scattering configuration. The simplest effect is e^+e^- pair creation by light. Even with a 50-GeV electron beam we are below energy threshold for this, if only one laser photon is involved. But if the laser beam is intense enough it becomes probable for pair creation to occur in the collision of several laser photons with a high-energy backscattered photon. The signal for this will be quite clean.

The fourth experiment is true light-by-light scattering into a two-photon final state. At the projected laser intensity, it is 3 times more probable that three laser photons rather than one be involved in the scattering process. This experiment is difficult in that the rates are somewhat low, and most of the scattered photons emerge at small angles to the incident high-energy photon beam.

Speculative interest in the above set of experiments has been stimulated by the possible production of an axion-like object in heavy-ion collisions.[2] The possbility of producing axions in the reaction $\gamma + e \rightarrow a + e$, followed by the decay $a \rightarrow e^+e^-$ (or $a \rightarrow \gamma\gamma$), has recently been raised by Brodsky *et al.*[8] Note that in the case of a multiphoton interaction with the electron, a higher-mass axion could be produced than with a single photon, so the kinematic limits mentioned in ref. 8 can

be substantially modified, depending on the laser intensity. Also note that a neutral axion of mass less than $2mc^2$ might be observed as a resonance in a light-by-light scattering experiment.

The proposed experiments are conceptually related to the possibility of spontaneous pair creation in strong magnetic fields, such as should exist at the surface of neutron stars. Considerations of the 'applied' effects of nonlinear QED have been made by several astrophysicists.[9−12]

1-3. Future Experiments.

As more intense lasers and higher energy electron beams become available one can explore more dramatic nonlinear effects. Only semiclassical theories exist for these effects, which have not been greatly pursued in the literature. An active experimental program would be a source of revitalization to the theoretical study of strong-field electrodynamics.

One effect which will become accessible is vacuum Čerenkov radiation.[13] Because of vacuum polarization in an intense electromagnetic field, the vacuum takes on an index of refraction. Hence the interaction of a fast electron with such a field should include a component of radiation with an angular distribution peaked at the Čerenkov angle. A similar effect may be observable when the strong field is probed by a high-energy photon: the traveling pulse of vacuum polarization which follows the probe photon which might lead to Čerenkov-like corrections to light-by-light scattering.

A more speculative effect is Unruh radiation, the non-gravitational equivalent of the Hawking radiation of a black hole.[1] The interaction of a highly accelerated electron with the vacuum fluctuations of the electromagnetic field may lead to a new type of radiation. This effect might become observable for 50-GeV electrons passing through a laser beam of 30 times the field strength of the proposed laser. (Coincidentally this is also the approximate condition for the onset of the vacuum Čerenkov effect.)

An experiment to study the anomalous magnetic moment of the W boson is also possible.[14−16] For this the 37-GeV backscattered photon beam is brought into collision with a 50-GeV electron beam (at the SLC intersect). In the reaction $\gamma e \to W\nu$ the angular distribution of the W is quite sensitive to its magnetic moment. The rate for this process is somewhat low ($\sim$ one event per month, but $\sim$ one in three days if 60-GeV beams were available).

It has been suggested that some of the broken symmetries of the weak interac-

tion might be restored for particles in a strong electromagnetic field.[17−19] Certainly if field strengths

$$E = m_W^2 c^3/e\hbar \sim 6 \times 10^{26} \text{ V/cm}$$

could be achieved quite novel physics would become accessible. For more modest field strengths, people have also speculated as to observable changes in the rates for weak-interaction processes.[20−22]

Studies of nonlinear behavior of single particles in a strong background field have been enormously fruitful in condensed-matter physics, but are little pursued in experimental high-energy physics. The Higgs mechanism is a theoretical example of such behavior relevant to elementary-particle physics. While there are numerous efforts to locate a Higgs particle, there is no experimental effort devoted to exploration of effects of an extended Higgs field. The proposed program does not directly remedy this glaring oversight, but it will establish experimental methods to probe fundamental properties of macroscopic volumes of space-time under extreme conditions.

2. The Phenomenology of Nonlinear QED.

As remarked in section 1, nonlinear effects due to vacuum polarization arise when an electromagnetic field attains the critical strength†

$$E_{\rm crit} = m^2/e = 1.32 \times 10^{16}\ {\rm V/cm},$$

in the frame of some relevant observer. When such a field strength is to be provided by a focused laser beam, another type of nonlinearity is also prominent: multiphoton effects. Indeed, that latter must be understood experimentally before studies of vacuum polarization in strong laser beams can be interpreted. Sections 2-1 through 2-3 review the present understanding of multiphoton effects in the interaction of a free electron in an intense wave field. Then sections 2-4 through 2-8 discuss various effects of vacuum polarization which will be accessible to experiment. Section 2-9 speculates on the use of laser techniques to produce W bosons.

2-1. A Free Electron in an Intense Laser Beam.

2-1a. Classical Analysis.

The steady-state motion of an electron in a plane electromagnetic wave is a well-known problem in classical physics.[23] (The steady-state solution ignores the radiation reaction due to the scattering of the incident light by the electron.) The motion is especially simple in a frame in which the electron is at rest on the average. (This is *not* typically the lab frame, as discussed further below.) The case of a circularly polarized wave is also simpler than that of linear polarization. For circular polarization, the electromagnetic field vectors **E** and **B** have constant magnitude and, in a fixed plane perpendicular to the direction of wave propagation, rotate at the angular frequency ω of the wave. The motion of the electron is then simply in a circle at anglular velocity ω, with the electron velocity **v** always parallel to **B**. Allowing for the possibility of relativistic velocities, $\mathbf{F} = m\mathbf{a}$ implies

$$\gamma_\perp m\omega^2 r = \gamma_\perp m\omega v = eE \qquad \text{where} \qquad \gamma_\perp = 1/\sqrt{1-{\beta_\perp}^2} \qquad \text{and} \qquad \beta_\perp = v/c.$$

Hence we may write‡

$$\gamma_\perp \beta_\perp = \frac{eE}{m\omega c} \equiv \eta,$$

† We will occasionally use units in which $\hbar = c = 1$.

‡ In plasma physics the quantity $eE/m\omega c$ is often called $v_{\rm osc}/c$. As we are particularly interested in the regime where the value of this quantity exceeds 1, we adopt the new notation, η.

leading to

$$\gamma_\perp = \sqrt{1+\eta^2} \qquad \text{and} \qquad \beta_\perp = \eta/\sqrt{1+\eta^2}.$$

The radius of the electron's orbit is

$$r = \frac{eE}{\gamma_\perp m\omega^2} = \frac{\eta}{\sqrt{1+\eta^2}}\frac{\lambda}{2\pi} \le \frac{\lambda}{2\pi},$$

where λ is the wavelength of the electromagnetic wave.

For waves with other than circular polarization it is convenient to define

$$\eta^2 \equiv \frac{e^2\langle E^2\rangle}{m^2\omega^2c^2},$$

where the average is with respect to time. Then (most) expressions involving η deduced for the case of circular polarization will hold for all types of polarization.

> For linearly polarized waves the path of the electron is a 'figure 8,' with the plane of the orbit containing **E** and the wave vector **k**. The transverse oscillation of the electron is at frequency ω and has r.m.s. amplitude equal to r as stated above in terms of η. The longitudinal oscillation of the electron is at frequency 2ω, and has amplitude $\eta/(4\sqrt{2}\sqrt{1+\eta^2})$ times the transverse amplitude.

It is interesting to note that for a plane wave, the dimensionless parameter η is a relativistic invariant of the electromagnetic field:†

$$\eta = \frac{e}{mc^2}\sqrt{-A_\mu A^\mu},$$

where A_μ is the 4-vector potential of the wave.

We will find that multiphoton interactions between the electron and the electromagnetic wave become important once $\eta \gtrsim 1$, *i.e.*, once the motion of the electron in the wave field is relativistic. It is useful to record some numerical relations between η, the electric field strength E, and the wave intensity I. First note that

$$I\ [\text{watts/cm}^2] = \frac{\langle E^2\rangle}{377\ [\text{ohms}]} \qquad \text{for } E \text{ in V/cm.}$$

Hence

$$E_{\text{r.m.s.}}\ [\text{V/cm}] = 19.4\sqrt{I\ [\text{watts/cm}^2]}.$$

Then we find

$$\eta^2 = 3.7\times10^{-19} I\lambda^2 \qquad \text{for } I \text{ in watts/cm}^2 \text{ and } \lambda \text{ in } \mu\text{m.}$$

† We use a metric such that $A_\mu A^\mu = A_0^2 - \mathbf{A}^2$.

For example, with $\lambda = 1.05$ μm ($\hbar\omega = 1.17$ eV), as in the proposed experiment, $\eta = 1$ corresponds to intensity $I = 2.4 \times 10^{18}$ watts/cm^2, and in turn to an electric field strength of $E = 3 \times 10^{10}$ V/cm. At the focus of a diffraction-limited laser beam the intensity is related to the beam power by $I \sim P/(2\pi\lambda^2)$, so we have the approximate result

$$\eta^2 \sim 5 \times 10^{-12} P[\text{watts}],$$

independent of the laser wavelength.

The expression for the radius r of the electron's orbit allows us to determine the range of applicability of the classical picture, namely that r be much greater than the Compton wavelength of the electron, $\hbar/mc$. This implies that $\eta/\sqrt{1+\eta^2} \gg \hbar\omega/mc^2$ must hold in the frame in which the electron is at rest on the average. Anticipating the case when the wave field is probed by an electron with Lorentz factor $\gamma_\parallel$ before it meets the wave, the restriction becomes $\eta/\sqrt{1+\eta^2} \gg \gamma_\parallel \hbar\omega/mc^2$ in terms of lab quantities. We see that strictly speaking there is no weak-field ($\eta \ll 1$) classical limit because r is too small.† Happily this does not invalidate the textbook derivations of Thomson scattering (because the 'classical' electron radius is actually the quantum mechanical parameter α/m in units where $\hbar = c = 1$). For example, a wave of 1 eV photons incident on an electron at rest must have $\eta \gtrsim 10^{-5}$ for the classical path to have meaning. This corresponds to a wave intensity of $\gtrsim 10^8$ watts/cm^2, which was hard to achieve before the development of the laser.

We also note that there is no classical limit when $\gamma_\parallel \hbar\omega \gtrsim mc^2$; then the wavelength of the light appears shorter than a Compton wavelength in the electron's rest frame. This is of course the condition which led to the distinction between Thomson scattering and Compton scattering. We pursue the case of strong fields with short wavelengths in section 2-3.

2-1b. The Mass Shift Effect.

For an electron executing the relativistic, classical motion found above, we

† Note another paradox: The oscillatory motion of the electron requires continuous change in its momentum components transverse to the momentum of the wave. Hence there must be continuous emission and absorption of virtual photons (which carry momentum but not energy) which interact with a distant boundary. The physical significance of the distant boundary is much less clear for a wave field than for, say, a d.c. magnetic field which has trapped an electron in a cyclotron orbit.

readily see that the mass of the electron is increased to $\overline{m}$ where

$$\overline{m} = \gamma_\perp m = m\sqrt{1+\eta^2}.$$

The mass increase is due to the transverse oscillation of the electron at frequency ω, and the amplitude of the oscillation is always less than the wavelength λ. Thus when considering scattering of the incident light by the electron, the light cannot resolve the details of the oscillatory motion; the scattering process can be affected by this motion in only an average way. In effect, the electron doesn't appear to oscillate, but simply has the shifted mass $\overline{m}$ found above. For example, in the kinematics of a scattering process, we must use an effective 4-vector for the electron with invariant mass $\overline{m}$ rather than m, as described in the next section.

Although we have motivated the mass shift classically, it was first noted in solutions to the Dirac equation for electrons in a plane electromagnetic wave.[24−26] It has never been observed experimentally.

2-1c. The Drift Velocity.

Thus far we have considered only the oscillatory motion of the electron due to a plane wave in the frame in which the electron is at rest on the average. However if an electromagnetic wave is incident on an electron initially at rest the subsequent motion is not purely oscillatory. The electron also takes on a 'drift' velocity along the direction of wave propagation, which can be large when $\eta \gtrsim 1$.[27] The drift velocity is the result of transient effects when the electron first encounters the field. During this time the electron's motion is not perfectly in phase with the wave and the $\mathbf{v} \times \mathbf{B}$ force has a component in the direction of the wave propagation.

We can avoid detailed consideration of the transient behavior and calculate the drift velocity of the electron once steady motion is established by thinking of the reaction in terms of photons. The argument which led to the relation $\overline{m} = m\sqrt{1+\eta^2}$ was made in the frame in which the drift velocity of the electron vanishes. However this frame is not necessarily the lab frame. In the general case suppose p_μ is the 4-momentum vector of the electron in the lab frame before entering the wave, and ω_μ is the 4-vector of a wave photon in the lab. Then $\overline{p}_\mu$, the effective 4-vector of the electron in the wave, must have the form

$$\overline{p}_\mu = p_\mu + \epsilon\omega_\mu,$$

where the value of ϵ is to be determined. We know that

$$\overline{p}^2 = \overline{m}^2 = m^2 + \eta^2 m^2$$

Hence

$$\epsilon = \frac{\eta^2 m^2}{2 p_\mu \omega^\mu}.$$

For example, if the electron is initially at rest,

$$p_\mu = (m, 0, 0, 0), \qquad \omega_\mu = (\omega, 0, 0, \omega),$$

so that

$$p_\mu \omega^\mu = m\omega \qquad \text{and hence} \qquad \epsilon = \frac{\eta^2 m}{2\omega}.$$

Then

$$\overline{p}_\mu = \left(m(1 + \eta^2/2), 0, 0, \eta^2 m/2\right).$$

The drift velocity is thus

$$\beta_\parallel = \eta^2/(2 + \eta^2).$$

It is tempting to interpret the paramter ϵ as the number of wave photons absorbed (without re-emission) by the electron as it enters the wave. This cannot be strictly correct, as seen from a consideration of angular momentum. In a circularly polarized wave, the circular motion of an electron, found above, corresponds to angular momentum

$$L = \gamma_\perp m v r = \frac{\eta^2 m c^2}{\omega\sqrt{1 + \eta^2}}.$$

However, if the electron had simply absorbed ϵ wave photons, its angular momentum would then be $\epsilon = \eta^2 m c^2/(2\omega)$. For $\eta \ll 1$ the electron appears to absorb 2 units of angular momentum for each quantum of energy taken from the wave. We surmise that the electron actually absorbs a larger number of wave photons than ϵ and then radiates away energy (and some angular momentum) in the form of soft photons during the transient phase. Indeed, this must happen if the properties of an electron in a wave ($\overline{m}$, $\beta_\parallel$, L, etc.) can take on continuous values, as suggested by the classical arguments.†

† An analogous situation occurs in the a.c. Stark effect–the shift of atomic energy levels in a wave field. The size of the level shift is not restricted to integer multiples of the wave photon energy. Again this is only possible if the atoms absorb wave photons, and then radiate away the energy difference between the absorbed energy and the eventual energy shift. This low frequency radiation occurs only during the transient phase, and would be undetected in ordinary atomic physics experiments.

It may be amusing to note the field intensity for which the electron mass shift is equal to the energy of a wave photon, namely $\eta^2 = 2\omega/m$. For the proposed laser, $\lambda = 1.05$ μm corresponds to $\omega = 1.17$ eV, which leads to $\eta^2 \sim 5 \times 10^{-6}$, $I \sim 10^{13}$ watts/cm^2, and $E \sim 6 \times 10^7$ V/cm. It is perhaps no coincidence that nonlinear ionization processes become important when atoms are placed in even such 'low-strength' waves.[28]

2-1d. The Need for Relativistic Electrons.

In practice it is doubtful that a free electron which is initially at rest can occupy the focus of an intense laser beam. The electron will be expelled from the strong field region by the 'ponderomotive' or 'field-gradient' force.[29,30] This force arises during the transient phase when the electron absorbs energy and momentum from the wave, while shifting its mass from m to $\overline{m}$.

A sense of the field-gradient force can be gotten from a non-relativistic argument. The effective mass $\overline{m}$ can be thought of as describing an effective potential for the electron inside the wave field:

$$U_{\text{eff}} = \overline{m}c^2 = mc^2\sqrt{1+\eta^2} \sim mc^2 + \tfrac{1}{2}mc^2\eta^2.$$

Hence

$$\mathbf{F} = -\nabla U \sim -\tfrac{1}{2}mc^2\nabla\eta^2 = -\frac{2\pi e^2}{m\omega^2 c}\nabla I$$

where I is the intensity of the wave. In a focused laser beam the intensity has a strong transverse gradient which will push an electron away from the optical axis. In a pulsed beam the field-gradient force will also push an electron away from the leading and trailing edges of the pulse.

Another view of this effect is obtained by analogy to the reflection of low frequency light off of an electron plasma. From the dispersion relation for light in a plasma,

$$\omega^2 = k^2c^2 + \omega_p^2 \qquad \text{where } \omega_p = \text{plasma frequency},$$

we infer that a photon inside the plasma has an effective mass given by

$$m_{\text{eff}}^2 = \left(\hbar\omega_p/c^2\right)^2.$$

For an electron in an intense photon beam we found a mass shift of $\Delta m^2 = \eta^2 m^2$. If we consider the laser beam as a kind of 'plasma' of photons then we see that the quantity which plays the role of the plasma frequency is $\eta mc^2/\hbar$. Just as

photons with $\omega < \omega_p$ can't penetrate an electron plasma, we infer that electrons with momentum less that ηmc can't penetrate a photon beam. Thus electrons with initial velocities such that $\gamma\beta < \eta$ will be expelled from the strong field region of the laser beam.

The conclusion is that intense laser beams can only be probed by relativistic electrons.

2-2. Nonlinear Thomson Scattering.

2-2a. Classical Analysis.

If an electron is placed in a wave of field-strength $\eta = eE/m\omega c \gtrsim 1$, it achieves relativistic velocities during its transverse oscillation. This oscillation generates all orders of multipole moments, but the radiation due to the n^{th} order moment is smaller than dipole radiation by a factor of order $(v/c)^{2n-2}$.[31] Recall that the frequency of the n^{th} order multipole radiation is at the n^{th} harmonic of the driving wave frequency (in the frame in which the electron is at rest on average). Thus when $\eta \sim 1$ multipole radiation at higher harmonic frequencies becomes comparable to that of dipole radiation.

If we divide that radiated intensity by the energy flux of the incident wave we obtain the scattering cross section. For scattering into the fundamental frequency, the cross section is of course

$$\sigma_{\text{Thomson}} = \tfrac{8\pi}{3} r_o^2,$$

where r_o is the classical electron radius. Then the cross section for scattering into frequency $n\omega$ varies approximately as

$$\sigma_{n\omega} \sim \sigma_{\text{Thomson}} \eta^{2n-2} \sim r_o^2 \eta^{2n-2} \qquad \text{for } \eta \lesssim 1.$$

These arguments can be expressed in terms of photons by noting that radiation at frequency $n\omega$ corresponds to absorption of n photons by the electron followed by emission of one photon at frequency $n\omega$. A simple QED estimate of the cross section would be

$$\sigma_{n\omega} \sim \frac{\alpha^{n+1}}{m^2} = \alpha^{n-1} r_o^2$$

counting one power of α for each external photon, and noting $r_o = \alpha/m$. On comparison with our classical argument we reach an important conclusion. In strong fields where a QED approach is necessary ($E > m^2/e$), there is a second dimensionless expansion parameter which depends on e^2 besides α, namely η^2. Thus we

anticipate that a detailed QED analysis of higher harmonic radiation in the regime $\eta \gg 1, E > m^2/e$ cannot be done via (a finite number of) Feynman diagrams, but must involve nonperturbative techniques.

Detailed classical considerations of higher harmonic radiation were first made by Schott.[32] If his equation (157), p. 125, for the radiated intensity is converted to a cross section, we find

$$\frac{d\sigma_{n\omega}}{d\cos\theta} = \frac{4\pi n r_o^2}{\eta^2}\left(\cot^2\theta\, J_n^2(n\beta\sin\theta) + \beta^2 J_n'^2(n\beta\sin\theta)\right),$$

where θ is the scattering angle. In this we have divided the usual expression by n so the cross section is a measure of the number of photons produced at frequency $n\omega$, rather than of scattered energy. In making rate estimates for the proposed experiment we will use a more general expression, applicable to nonlinear Compton scattering, presented in section 2-3 below.

In the extreme relativisitic limit, $\eta \gg 1$, Schott's result is equivalent to the standard expression for synchrotron radiation. We discuss this limit in section 2-2d. In the weak field limit, $\eta \ll 1$, we note that $\eta \sim \beta$ and that $J_n(n\beta\sin\theta) \sim (\frac{1}{2}n\beta\sin\theta)^n$, which leads to $\sigma_{n\omega} \sim r_o^2\eta^{2n-2}$ as claimed above.

2-2b. The Frequency of the Scattered Light.

In the multiphoton scattering process

$$n\omega + e \to \omega' + e',$$

the frequency of the scattered light, ω', is modified by the mass-shift effect for incident waves with $\eta \gtrsim 1$, as well as usual kinematic considerations. To quantify this change we write energy-momentum conservation for the reaction in terms of 4-vectors:

$$n\omega_\mu + \overline{p}_\mu = \omega'_\mu + \overline{p}'_\mu.$$

Noting that $\overline{p}'^2 = \overline{m}^2$ we find

$$n\omega'_\mu\omega^\mu + \omega'_\mu\overline{p}^\mu = n\omega_\mu\overline{p}^\mu.$$

For example, if the electron is initially at rest† and we write

$$\omega'_\mu = (\omega',\ \omega'\sin\theta,\ 0,\ \omega'\cos\theta)$$

† Although we found in section 2-1d that an electron initially at rest is not a suitable probe of a strong wave, it serves to introduce the frequency shift due to the mass-shift effect.

then we find

$$\omega' = \frac{n\omega}{1 + \left(\frac{n\omega}{m} + \frac{\eta^2}{2}\right)(1 - \cos\theta)}.$$

This is the appropriate form of the Compton-scattering relation for high field strengths.

If we scatter optical photons off electrons then $\omega/m \lesssim 10^{-5}$ which is negligible as usual. But η^2 is large when there is significant probability for higher harmonic radiation. In this case there is substantial variation of the frequency ω' with scattering angle. This effect occurs for the fundamental harmonic ($n = 1$) as well. Measurement of the frequency shift with angle allows a direct determination of the parameter η^2, independent of the intensities of the various higher harmonics. This feature will aid greatly in the interpretation of experimental results.

In the mid 1960's a small controversy arose as to the observability of the electron mass shift and of the frequency shift of the scattered photon. Although these are essentially classical effects, there is some difficulty in demonstrating them in a QED approach. This arises because QED calculations for strong fields can only be made at present for plane waves of infinite extent and duration. Reasonably convincing arguments show that the QED calculations indeed have the proper classical limit in the case of pulsed fields.[30,33,34] The conclusion remains that the photon frequency shift should be detectable, even if its value is not exactly that given by arguments based on plane waves.

2-2c. The Possibility for Experiment.

The program of a possible experiment is now reasonably clear. The key is the production of a laser beam for which the field strength satisfies $\eta = eE/m\omega c \gtrsim 1$. We anticipate that in practice this can be obtained only by focusing the beam, and that for a diffraction-limited focus the condition $\eta \sim \eta_{\max}$ can be maintained only over a volume $\sim \lambda^3$. The beam then scatters off any electrons in this volume leading to a discrete spectrum of radiation at any fixed angle. For fields with strength $\eta \sim 1$ the target electrons must have relativistic velocities, which leads to substantial Doppler shifts in the scattered light. In addition, the observed frequency of each harmonic will be lower than that expected for weak fields, due to the mass-shift effect. The experiment should detect this frequency shift, as well as measure the intensity of the various harmonics of the scattered light.

A rate estimate for the nonlinear-Thomson-scattering experiment can be made

by recalling the Larmor formula,†

$$\frac{dU}{dt} \sim \frac{e^4 E^2}{m^2}.$$

Because of the small focal volume any one electron will experience the strong field only for a few optical cycles. The energy radiated in one cycle of the wave is

$$dU \sim \frac{e^4 E^2}{m^2 \omega} \text{ per cycle,}$$

and the number of photons radiated is

$$dN = \frac{dU}{\omega} \sim \frac{e^4 E^2}{m^2 \omega^2} \sim \alpha \eta^2 \text{ photons/cycle.}$$

This rate is of course to be multiplied by the number of electrons in volume λ^3. Thus once fields with $\eta \sim 1$ have been achieved the scattering rate is quite substantial.

Nonlinear effects have been observed in the scattering of light from a CO_2 laser or a Nd:glass laser off an electron plasma, where up to the 46th harmonic has been observed.[35–37] In these experiments the laser beam induces a sharp density gradient on the plasma which then supports nonlinear plasma oscillations leading to higher harmonic radiation. This effect is to be distinguished from present concerns of scattering off a single electron. In particular the electron mass shift and attendant frequency shift of the scattered photon have not been observed in the plasma experiments.

There appears to be only one previous study of higher harmonic radiation in the interaction of a free electron with a laser beam.[38] In this experiment laser pulses of 1.05-μm wavelength and intensity $\sim 2 \times 10^{14}$ watts/cm^2 were brought into collision with a beam of electrons whose energy could be varied from 0.5 to 1.6 keV. The electron density in the beam was about 10^{10}/cm^3. The field-strength parameter η was about 0.01, while the electron velocities ranged from 0.04 to 0.08 of c; hence the electron beam was not greatly perturbed by the field-gradient effect of the laser pulse. A small, but significant amount of second-harmonic radiation was observed, although η was too small for the η-dependent frequency shift to be detected, compared to the Doppler shift due to the moving target of electrons.

† While the follwing argument is made in the frame in which the electron is at rest on the average, the conclusion is clearly invariant under the choice of frame.

2-2d. Very Strong Fields.

This section is an aside on the case when the wave field is so strong that $\eta \gg 1$, which should become relevant in the near future.

Consider a circularly polarised wave of frequency ω incident head on with an electron with Lorentz factor γ. If the electron is not to be badly deflected by the wave then we need $\gamma \gg \eta$ according to section 2-1d. Following an analysis like that of section 2-1c we find that the energy of the electron once inside the wave remains γm to first order in η/γ. Of course much of this energy is in the transverse motion of the electron, so its longitudinal velocity has been decreased. This is described by the effective mass according to $\gamma m = \gamma_{\|}\overline{m}$. Since $\overline{m} = m\sqrt{1+\eta^2} \sim m\eta$ we have that $\gamma_{\|} \sim \gamma/\eta$. On transforming to the average rest frame of the electron the wave has frequency $\omega^\star \sim 2\gamma_{\|}\omega \sim 2\gamma\omega/\eta$. In this frame the electron is not at rest but moves in a circle at relativistic velocities, described by the Lorentz factor $\gamma_\perp = \overline{m}/m \sim \eta$. The radiation of the circling electron can be thought of as synchrotron radiation. From a classical analysis of the latter we know that the spectrum peaks at frequency $\omega^{\star\prime} \sim \gamma_\perp^3\omega^\star \sim \eta^3\omega^\star$, corresponding to maximum strength for the harmonic with $n \sim \eta^3$. This radiation is strong only in the plane of the circular motion (in the average rest frame of the electron). On transforming back to the lab frame, the radiation has characteristic frequency $\omega' = \gamma_{\|}\omega^{\star\prime} \sim \gamma\eta^2\omega$, and lies in a narrow cone of half angle $\sim \eta/\gamma$.

For strong enough wave fields the resulting radiation will include e^+e^- pairs and a classical analysis no longer suffices. The threshold for this QED correction is that the energy of the radiated photon as viewed in the average rest frame of the electron is equal to $2\overline{m}$. The critical energy is $\overline{m}$ and not m as any pairs produced must have the energy of the transverse oscillations of electrons in the strong field. The condition $\omega^{\star\prime} \gtrsim \overline{m}$ transforms to lab frame quantities as $\gamma\eta\omega \gtrsim m$ or $\gamma E \gtrsim m^2/e$ recalling that $\eta = eE/m\omega$. Not surprisingly, this is just the condition that the electric field in the true rest frame of the electron be stronger than the critical field introduced in section 1. Then the electron probes the wave field so as to stimulate pair creation as discussed in section 2-4 below.

2-2e. Comparison with Radiation in an Undulator.

This section is another aside to help place nonlinear Thomson scattering in the broader context of contemporary electrodynamic studies.

The phenomenon of nonlinear Thomson scattering is closely related to the

production of higher harmonic radiation in the passage of an electron through a static but spatially oscillating magnetic field.[39] In the analysis of an 'undulator' or 'wiggler' magnet of periodicity λ_o one introduces the dimensionless parameter $\eta = eB\lambda_o/2\pi mc^2$, where B is the r.m.s.-spatial-average magnetic field. For example, the radiation emitted in the forward direction has wavelength $\lambda \sim 2\lambda_o/\gamma_{\|}^2 = 2\lambda_o(1+\eta^2)/\gamma^2$ where γ is the Lorentz factor of the incident electron. Although the total velocity of the electron is unaffected by the undulator, its longitudinal component is reduced to compensate for the transverse oscillations. This leads to the appearance of η in the expression for λ. For $\eta \gtrsim 1$ the oscillations are strong enough that higher harmonic radiation is probable. The higher radiation has been observed,[40] and is considered a background to the operation of undulators as free-electron lasers, where it is desired to amplify only one frequency. Coherent production of higher harmonic radiation has been observed from a bunched electron beam obtained in an optical klystron.[41]

The magnetic field of the undulator can be thought of as consisting of virtual photons. In the lab frame these carry momentum h/λ_o but no energy. However in the average rest frame of a relativistic electron inside the undulator the virtual photons appear very much like real photons. If we wish to describe the radiation process as a kind of Thomson scattering off the virtual photons we must note that the electron takes on an effective mass $\overline{m} = m\sqrt{1+\eta^2}$ inside the undulator, so that $\gamma m = \gamma_{\|}\overline{m}$. As for the case of an electron in a laser beam, the 'mass-shift' effect is an artifice of a description which emphasizes the longitudinal motion of the electron and averages over the transverse oscillations.

2-3. Nonlinear Compton Scattering.

When a beam of electrons of energy γm is brought into head-on collison with a laser beam of frequency ω, in the average rest frame of the electron the incident light has frequency $2\gamma\omega$ (if γ is large compared to the field-strength parameter η). Then if $\gamma\omega \gtrsim m$ quantum corrections become important in the scattering process, and the nonlinear Thomson scattering is better described as nonlinear Compton scattering. Several authors have considered the quantum corrections to strong-field electron-photon scattering.[20,21,25,27,42–45] We find the work of Narozhny, Nikishov and Ritus[21] especially useful for computations.

Consider the absorption by an electron of n photons of frequency ω with the emission of a single photon of frequency ω' in the reaction

$$n\omega + e \rightarrow \omega' + e'.$$

We write energy-momentum conservation in terms of 4-vectors as

$$n\omega_\mu + \overline{p}_\mu = \omega'_\mu + \overline{p}'_\mu,$$

where $\overline{p}_\mu$ is the effective 4-vector of an electron in a wave of strength η, as discussed in section 2-1c. Note that the final state electron has effective mass $\overline{m}$ corresponding to the continuum states of an electron in a strong wave field. The cross section for circularly polarized wave photons is[21]

$$\sigma_{n\omega} = \frac{2\pi r_o^2}{u_1\eta^2}\int_0^{u_n}\frac{du}{(1+u)^2}\Bigg\{-4J_n^2(z)+ \\ +\eta^2\left(2+\frac{u^2}{1+u}\right)\left(J_{n-1}^2(z)+J_{n+1}^2(z)-2J_n^2(z)\right)\Bigg\},$$

where

$$u=\frac{\omega_\mu\omega'^\mu}{\omega_\mu\overline{p}'^\mu}, \qquad u_1=\frac{2\omega_\mu\overline{p}^\mu}{\overline{m}^2}, \qquad u_n = nu_1, \qquad \text{and} \qquad z=\frac{2\eta\sqrt{u(u_n-u)}}{u_1\sqrt{1+\eta^2}}.$$

Narozhny *et al.* show that in the weak-field, high-frequency limit this expression reduces to the Klein-Nishina formula, while in the strong-field, low-frequency limit this becomes the Schott formula given in section 2-2a. The physical content of the full expression is simply to combine the quantum effects of Compton scattering with the semiclassical strong-field effects discussed in section 2-2.

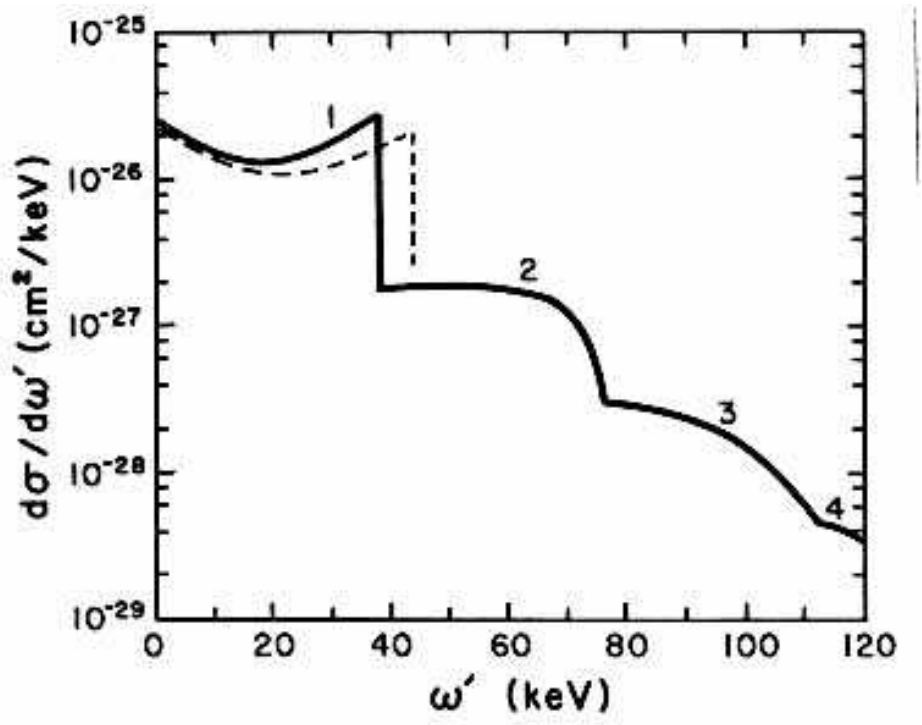

Figure 1. The differential cross section for nonlinear Compton scattering of 50-MeV electrons against a laser beam of 1.05-μm wavelength and field-strength parameter $\eta = 0.4$. The contribution due to the absorption of 1 through 4 laser photons is labeled. The dashed curve is the ordinary Compton cross section. Note the shift in the end point of the one-photon cross section.

In an experiment with highly relativistic electrons, the scattered photons of interest emerge with angles $\sim 1/\gamma$ with respect to the direction of the electron beam but with a broad range of energies. It is useful to express the differential scattering cross section as a function of the scattered photon energy, rather than the scattering angle. For this we relate the invariant u used above to the photon energy ω', and find†

$$\frac{du}{(1+u)^2} \sim \frac{d\omega'}{\gamma m} \qquad \text{if} \qquad \gamma \gg \eta.$$

Thus we may write

$$\frac{d\sigma_{n\omega}}{d\omega'} = \frac{2\pi r_o^2}{u_1 \eta^2 \gamma m} \left\{ -4J_n^2(z) + \eta^2 \left(2 + \frac{u^2}{1+u}\right) \left(J_{n-1}^2(z) + J_{n+1}^2(z) - 2J_n^2(z)\right) \right\}.$$

† It is helpful to evaluate the invariants in the center-of-mass frame, where u is a simple function of the scattering angle.

Figure 1 shows this cross section evaluated for electrons of 50 MeV and light of 1.05-μm wavelength with field-strength parameter $\eta = 0.4$, summed over the various numbers of absorbed photons. The contributions from 1 to 4 photon absorption can be resolved in the figure. The dashed curve is the Klein-Nishina cross section for comparison. In this example $\gamma\omega/m \sim 2\times10^{-4}$ so we are really dealing with Schott's classical result in comparison with Thomson scattering. Note however the shift in the 'Compton edge' from 44 keV down to 38 keV for scattering in the strong-field case.

The dependence of the scattered photon energy ω' on the laboratory scattering angle θ (defined with respect to the direction of the *electron* beam) may derived in a manner similar to that of section 2-2b. The result is

$$\omega' = \frac{4n\gamma^2\omega}{1 + 2\gamma^2(1-\cos\theta) + \left(\frac{2n\gamma\omega}{m} + \frac{\eta^2}{2}\right)(1+\cos\theta)}.$$

The maximum scattered photon energy occurs for $\theta = 0°$ (which is 180° backscattering from the point of view of the laser beam) and is

$$\omega'_{\max} = \frac{4n\gamma^2\omega}{1 + \eta^2 + \frac{4n\gamma\omega}{m}}.$$

These results exhibit the η-dependent frequency shift discussed in section 2-2b. For the example in Figure 1, $1 + \eta^2 = 1.16$, which leads to the shift of the Compton edge noted above.

Expressions for nonlinear Compton scattering with linearly polarized photons have been given by several authors,[27,42] but these are not as compact as for the case of circularly polarized light. The integrals needed for comparison with experiment could of course be performed on a computer.

2-4. Electron-Positron Pair Creation by Light.

Sections 2-4 through 2-8 discuss various phenomena would could be explored in extensions of the presently proposed experiment. Details of the latter appear in section 3.

2-4a. The Backscattered Photon Beam.

If the high-energy photons obtained from the backscatter of a laser beam off an electron beam are then brought into collision with a second laser beam we have a light-by-light scattering configuration. As the photon fluxes in a laser beam are

quite high there will be observable rates of light-by-light scattering, which has eluded direct experimental detection up to the present.†

While this proposal is primarily for the nonlinear-Thomson-scattering experiment, we digress here to discuss some features of the backscattered photon beam which would be used in the second-round experiments. This will be an upgraded version of the backscattered beam now in the C line at SLAC.[47−49]

It will be very advantageous to use a 50-GeV SLC beam, which could be transported in the C line if the field integrals of the momentum-selection dipoles and the permanent dump magnets are suitably increased. The instrumentation of the beam line would be upgraded to the standard of the SLC project.

The laser for the second-round experiments will operate at 0.308-μm wavelength (4.03 eV), as discussed in section 4. The endpoint energy of the backscattered photon beam is given by an expression such as that just mentioned in section 2-3:

$$\omega'_{\max} = \frac{4\gamma^2\omega}{1+\frac{4\gamma\omega}{m}} = \frac{E_e}{1+\frac{m^2}{4E_e\omega}},$$

where $E_e = \gamma m$ is the electron beam energy. Figure 2 sketches $\omega'_{\max}$ as a function of E_e for laser photons of wavelength 0.308 μm. For $E_e = 50$ GeV we have $\omega'_{\max} = 37.75$ GeV.

The backscattered photon beam then propagates some distance, taken here to be 20 m, and is brought into collision with another laser beam of 0.308-μm wavelength. To obtain the strongest nonlinear effects the latter laser beam will be focused to a spot of radius ~ 1 μm, close to the diffraction limit. Only those photons of the backscattered beam that pass through this rather small spot are of interest, and we refer to them as *the* backscattered beam in the following.

There are three measures of quality for the backscattered photon beam:

- high flux;
- nearly monochromatic energy spectrum;
- angular divergence $\lesssim m/\omega'$, which latter is characteristic of the light-by-light scattering of photons ω'.

---

† The production of electron-positron pairs by a photon in the field of a nucleus may be considered as a kind of light-by-light scattering, especially when one regards the nuclear Coulomb field as consisting of virtual photons.[46] Likewise, particle production via the collision of two virtual photons is now a common technique at electron-positron storage rings.

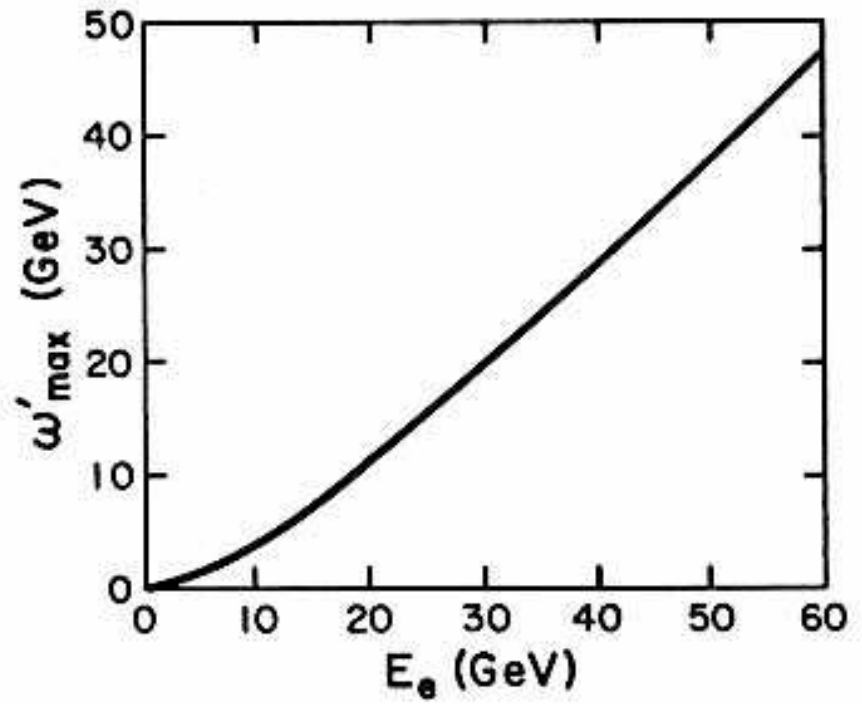

Figure 2. The maximum energy of the backscattered photon beam obtainable by colliding a laser beam of 0.308-μm wavelength against an electron beam of various energies.

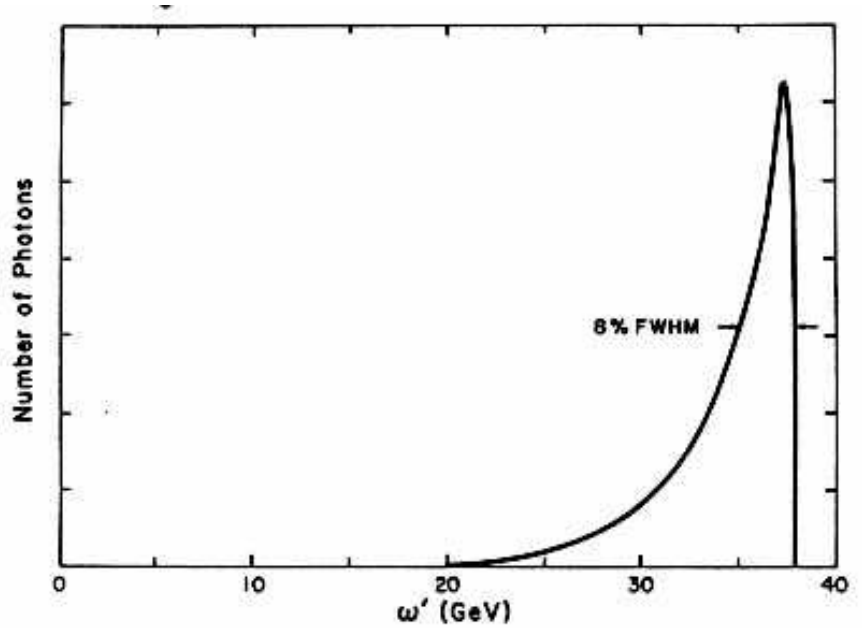

Figure 3. The energy spectrum of the backscattered photon beam obtained by colliding a laser beam of 0.308-μm wavelength against a 37-GeV electron beam.

All of these features depend on the radius of the electron beam at the production point of the backscattered beam. (We suppose the laser-beam size can always be adjusted to match that of the electron beam.) The angular divergence of the electron beam is related to the beam radius via the emittance, taken to be 3×10^{-8} cm-rad for an SLC beam. Then the flux of the backscattered beam (*i.e.*, that which passes through the 1-μm light-by-light scattering spot) is a slow function of the electron-beam radius, favoring a smaller radius. The backscattered beam is more monochromatic when the electron-beam divergence is small, favoring a large electron-beam radius. The divergence of the backscattered beam varies linearly with the electron-beam radius, favoring a small radius.

A reasonable compromise is an electron-beam radius of $\sim$ 50 μm. Then we estimate the flux of backscattered photons (as always, through the 1-μm light-by-light scattering spot) as about 3 per 10^{10} electrons for a laser pulse of 0.01 Joule energy. This supposes that the entire laser pulse passes through the $\sim$ 10-ps electron pulse, which is possible as a 50-μm-radius laser beam is well collimated. The calculated energy spectrum of the backscattered beam is shown in Figure 3, while the mean angular divergence of the beam is 3×10^{-6} rad.

2-4b. The Breit-Wheeler Process.

Light-by-light scattering becomes significant when the effects of vacuum polarization are large. This is often considered to occur in two different limits: low-intensity but high-frequency light; and for low-frequency but very intense light. In the proposed second-round experiments we would approach the high-frequency and high-intensity limits simultaneously, which requires a unified understanding of vacuum polarization processes.

Halpern[50] was the first to note that low-intensity light beams would scatter if the center-of-mass energy of a pair of colliding photons were similar to the electron mass. If ω_1 and ω_2 are the laboratory energies of the two photons which meet head on, this requires $\omega_1\omega_2 \sim m^2$. Breit and Wheeler[51] made the first calculation of a light-by-light scattering process, namely electron-positron pair creation by light, and found the cross section (near threshold) to be

$$\sigma_{\omega_1+\omega_2\rightarrow e^+e^-} \sim \pi r_o^2 \beta_{\rm cm},$$

where $\beta_{\rm cm}$ is the velocity of the electron or positron in the center-of-mass frame. Although this is actually a rather large cross section, the process has not been

observed due to lack of photon flux.†

Considerations of nonlinear electrodynamics in the strong-field limit arose following the statement of Klein's paradox[52] regarding the surprising behavior of the transmission coefficient when a Dirac electron encounters a steep potential barrier. Sauter[53] noted that an electric field is unstable against spontaneous electron-positron pair production if the potential gradient is greater than mc^2 across a Compton wavelength. This led to the critical field strength $E = m^2c^3/e\hbar$, introduced in section 1. Strictly speaking, an electromagnetic plane wave of arbitrary strength is stable against pair production, because a pair of massive particles can never have the same total 4-momentum as a photon.‡ Reiss[54] appears to have been the first to note the interesting possibility that if a strong electromagnetic wave is probed by a photon (or electron, *etc.*) pair creation may be likely, even though the center-of-mass energy of the probe photon plus a single wave photon is much less than the mass of the electron. Other treatments include refs. 21, 42, 44, and 55. Again we find ref. 21 especially useful for computations.

Pair creation in a strong wave field is described in terms of photons as

$$n\omega_1 + \omega_2 \to e^+e^-,$$

wherein n wave photons, ω_1, annihilate with the probe photon, ω_2, to produce the pair. This can of course also be considered as a multiphoton version of the Breit-Wheeler process. Following the argument of Sauter, this process becomes probable when the wave field strength approaches the critical field strength m^2/e in the rest frame of the e^+e^- pair. In this frame the probe photon has energy m (at threshold), so the Lorentz boost from the lab frame is $\gamma \sim \omega_2/2m$, assuming $\omega_2 \gg m$ in the lab frame. Hence the electric field strength of the wave in the e^+e^- rest frame is $\omega_2 E/m$, where E is the laboratory strength of the wave, and the wave and probe photons meet head on. The appropriate measure of field strength is then

$$\chi = \frac{\omega_2 E/m}{m^2/e} = \frac{\omega_1\omega_2}{m^2}\frac{eE}{m\omega_1} = \frac{\omega_{1\mu}\omega_2^\mu}{2m^2}\eta,$$

† Breit and Wheeler commented on the possible significance of their process to astrophysics. In present terms, cosmic ray photons of energies greater than $\sim 10^{16}$ eV will be attenuated due to scattering off the 3 °K microwave background radiation.

‡ A photon is stable against decay into an even number of photons according to charge-conjugation invariance, and stable against decay into an odd number of photons due to lack of phase space.

where η is the invariant $eE/m\omega c$ of a wave field introduced in section 2-1a. Parameter χ is a Lorentz invariant of the scattering process. Sauter showed that in weak fields the rate of pair production varies as $\exp^{-\pi/\chi}$. Even when $\omega_1\omega_2 \ll m^2$, pair production is likely, provided $\eta \gtrsim m^2/\omega_1\omega_2$.

For the detailed calculation of the cross section for the multiphoton Breit-Wheeler process, we express the reaction in terms of 4-momenta as

$$n\omega_{1\mu} + \omega_{2\mu} = \overline{p}_\mu + \overline{p}'_\mu.$$

Here $\overline{p}$ labels the electron and $\overline{p}'$ the positron. The use of $\overline{p}$ rather than p signifies that the electron and positron will be created as free-particle states in the strong wave field, and so have the shifted invariant mass $\overline{m}$ found in section 2-1b. Figure 4a sketches the classical paths of an electron and positron created with the threshold energy in a circularly polarized wave field. Because the particles must immediately assume the circular orbits discussed in section 2-1a, their effective mass is $\overline{m}$. For a pair created above threshold, the circular orbits become trochoids as sketched in Figure 4b. The cross section, for the case of circular polarization of both wave and probe photons, is found to be[21]

$$\sigma_{n\omega_1+\omega_2\to e^+e^-} = \frac{\pi r_o^2\, m^2}{\eta^2 \omega_{1\mu}\omega_2^\mu} \int_1^{u_n} \frac{du}{u\sqrt{u(u-1)}} \times \left\{ 2J_n^2(z) + \eta^2(2u-1)\left(J_{n-1}^2(z) + J_{n+1}^2(z) - 2J_n^2(z)\right)\right\},$$

where

$$u = \frac{\omega_{1\mu}\omega_2^\mu}{4\,\omega_{1\nu}\overline{p}^\nu\,\omega_{1\tau}\overline{p}'^\tau}, \quad u_o = \frac{\omega_{1\mu}\omega_2^\mu}{2\overline{m}^2}, \quad u_n = nu_o, \quad \text{and} \quad z = \frac{4\eta m\overline{m}}{\omega_{1\mu}\omega_2^\mu}\sqrt{u(u_n-u)}.$$

Conservation of energy requires that the number n of wave photons be greater than $1/u_o$ ($= \overline{m}^2/\omega_1\omega_2$ for head-on collisions). The field-strength parameter χ can be seen to enter the above by rewriting

$$z = \frac{2\eta^2\sqrt{1+\eta^2}}{\chi}\sqrt{u(u_n-u)}.$$

For weak fields ($\eta \ll 1$) the cross section for pair creation via one wave photon reduces to the Breit-Wheeler result.

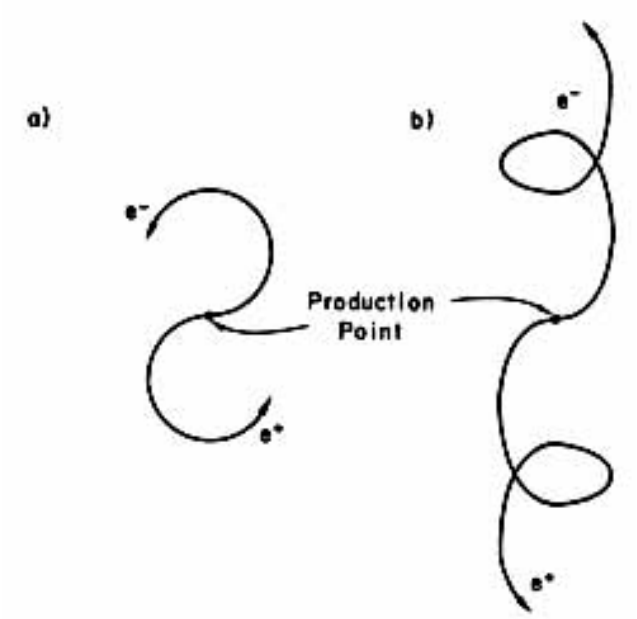

Figure 4. **a)** The trajectories of an electron-positron pair created with threshold energy in a strong wave field. The orbits are the circles discussed in section 2-1a; **b)** The trajectories for pair creation above threshold. The orbits are trochoids.

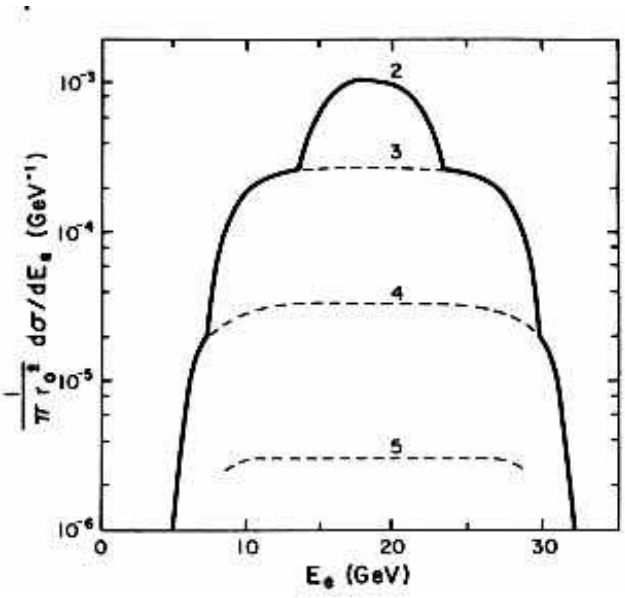

Figure 5. The cross section, normalized to πr_o^2, for the multiphoton Breit-Wheeler effect. The backscattered photon beam has energy 37 GeV. The laser beam has wavelength 0.308 μm and field-strength parameter $\eta = 0.25$. The reaction is energetically forbidden to proceed with only one laser photon. The contributions to the cross section from 2 through 5 laser photons are labeled.

As in section 2-3, it is useful to note that the invariant u is a simple function of the cosine of the scattering angle in the center-of-mass frame. This allows us to write†

$$\frac{du}{u\sqrt{u(u-1)}} \sim \frac{2dE_e}{\omega_2} \qquad \text{when} \qquad \omega_2 \gg n\omega_1,$$

where E_e is the laboratory energy of the final-state electron. Hence we find the differential cross section for a head-on collision to be

$$\frac{d\sigma_{n\omega_1+\omega_2\to e^+e^-}}{dE_e} = \frac{\pi r_o^2\, m^2}{\eta^2\omega_1\omega_2^2}\left\{2J_n^2(z) + \eta^2(2u-1)\left(J_{n-1}^2(z) + J_{n+1}^2(z) - 2J_n^2(z)\right)\right\}.$$

Figure 5 shows a plot of this cross section for beam parameters suitable for the second-round experiments. The backscattered photon beam (section 2-4a) of endpoint energy 37 GeV is brought into collsion with a second laser beam, also of wavelength 0.308 μm, and field-strength parameters $\eta = 0.25$, and $\chi = 0.29$. It is not energetically possible to produce electron-positron pairs with a single such laser photon,‡ but with two laser photons the process is allowed. In Figure 5 the contributions to pair production from 2, 3, 4 and 5 laser photons are sketched. Thus if any e^+e^- pairs are observed they will be the result of two simultaneous nonlinear effects: vacuum polarization and multiphoton interactions.

Figure 6 shows how the total pair-production cross section varies with the energy ω_2 of the backscattered photon beam, always supposing that it collides with a laser beam of 0.308-μm wavelength and field-strength parameter $\eta = 0.25$. Figure 7 illustrates how the total pair-production cross section varies with field-strength parameter η for a fixed beam energy $\omega_2 = 37$ GeV and a fixed laser wavelength of 0.308 μm. In this case the invariant χ is simply related by $\chi = 1.14\eta$. Once $\chi \gtrsim 1$ the cross section ceases to rise, but then pair production has become a high-rate process. It is amusing to note that for the case of $\eta = 4$ in Figure 7 the mean number of laser photons annihilated in the pair creation is predicted to be 60.

In the second-round experiment, the rate of multiphoton pair creation would be about one event per 300 pulses of 3×10^{10} electrons (~ 10 backscattered photons). For this, Figure 6 indicates that the total cross section at $\omega_2 = 37$ GeV is about

---

† We use a factor 2 rather than 4, as we wish to consider E_e varying from $E_{e,\min}$ to $E_{e,\max}$, instead of from $\omega_2/2$ to $E_{e,\max}$ which latter corresponds to $1 \le u \le u_n$.

‡ The threshold energy of the probe photon is $\omega_2 = 65$ GeV, which could be produced in the backscatter of a 78-GeV electron beam against the 0.308-μm-wavelength laser beam.

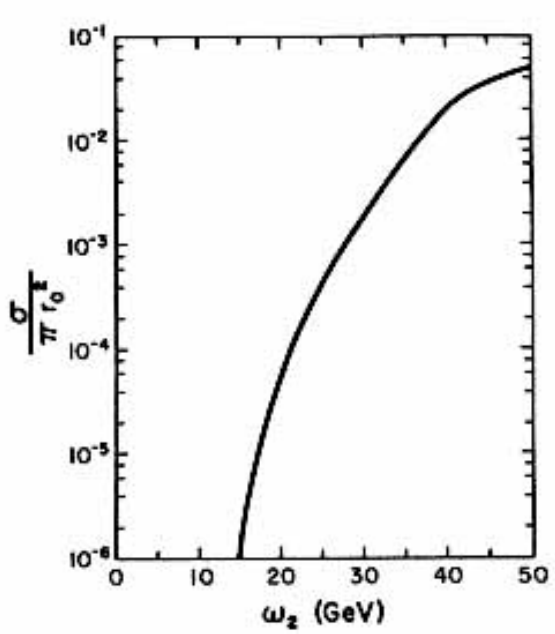

Figure 6. The cross section for the multiphoton Breit-Wheeler process as a function of the energy of the backscattered photon beam, for collisions with a laser beam of wavelength 0.308 μm and field-strength parameter $\eta = 0.25$.

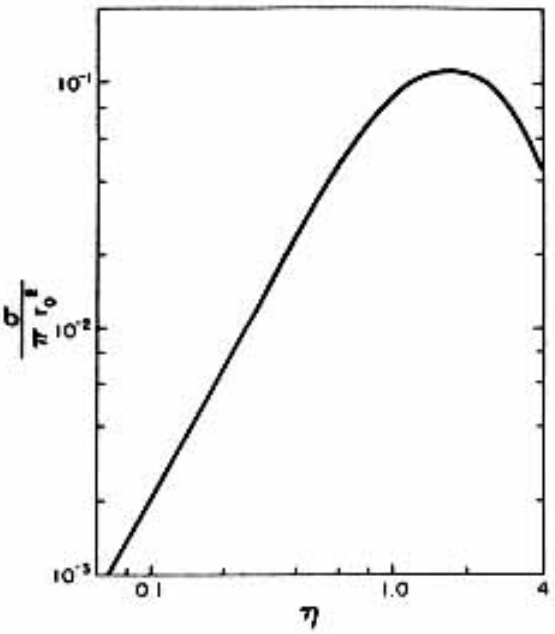

Figure 7. The cross section for the multiphoton Breit-Wheeler process as a function of the field-strength parameter η of a laser beam of 0.308-μm wavelength, in collision with a 37-GeV backscattered photon beam.

$0.01\pi r_o^2 \sim 3 \times 10^{-27}$ cm^2. We take the energy of the second laser pulse to be 0.2 Joule, corresponding to 3×10^{17} photons. When this beam is focused to a spot of 1-μm radius the depth of focus is only about ± 20 μm, so the strong-field region is only about 1% of the length of the backscattered photon bunch (10 ps $\Rightarrow$ 3 mm). Then for one pulse,

$$\text{No. of events} = \frac{\sigma \cdot N_{\omega_1} \cdot N_{\omega_2} \cdot \text{overlap}}{\text{beam area}} \sim \frac{3 \times 10^{-27} \cdot 3 \times 10^{17} \cdot 10 \cdot 10^{-2}}{3 \times 10^{-8}} \sim 0.003.$$

The cross section for pair production by linearly polarized photons has also been calculated,[42,54] but again the result is not as compact as for the case of circular polarization. When $\eta \gg 1$, there is a threshold suppression of pair creation via circularly polarized photons compared to that by linearly polarized photons, because in the former case the leptons are created in states of high angular momentum.[55] Asymptotic forms for the cross sections for pair production by both circularly and linearly polarized photons are available in the limit $\eta \gg 1$.[54,55] Other suggestions to study pair creation with laser light include refs. 56-58.

2-5. Light-by-Light Scattering.

The first calculation of elastic light-by-light scattering,

$$\omega_1 + \omega_2 \rightarrow \omega_3 + \omega_4,$$

was made in the low-frequency limit by Euler and Kockel,[59] followed by the work of Achieser[60] in the high-frequency limit. Karplus and Neuman[61] gave the first treatment applicable to all frequencies, but still in the low-intensity limit. There appears to be nothing in the literature concerning light-by-light scattering for strong fields (such that field-strength parameter $\eta \gtrsim 1$), although the work of Becker and Mitter[62] may provide a starting point. As remarked earlier, light-by-light scattering of real photons has never been observed experimentally.

For low frequencies the light-by-light scattering cross section rises as $\approx 0.13(\omega_1\omega_2/m^2)^3$ μb, while at high frequencies it falls as $\approx 20m^2/(\omega_1\omega_2)$ μb. The peak cross section occurs for $\omega_1\omega_2 \approx 2.25m^2$, and is about 1.6×10^{-30} cm^2. The behavior of the cross section is sketched in Figure 8, reproduced from a paper by de Tollis.[63] The low-frequency approximation is seen to be quite good up to $k \equiv \sqrt{\omega_1\omega_2}/m \sim 0.7$, while at $k = 1$ the actual cross section is about 10 times the extrapolation of the low-frequency result.

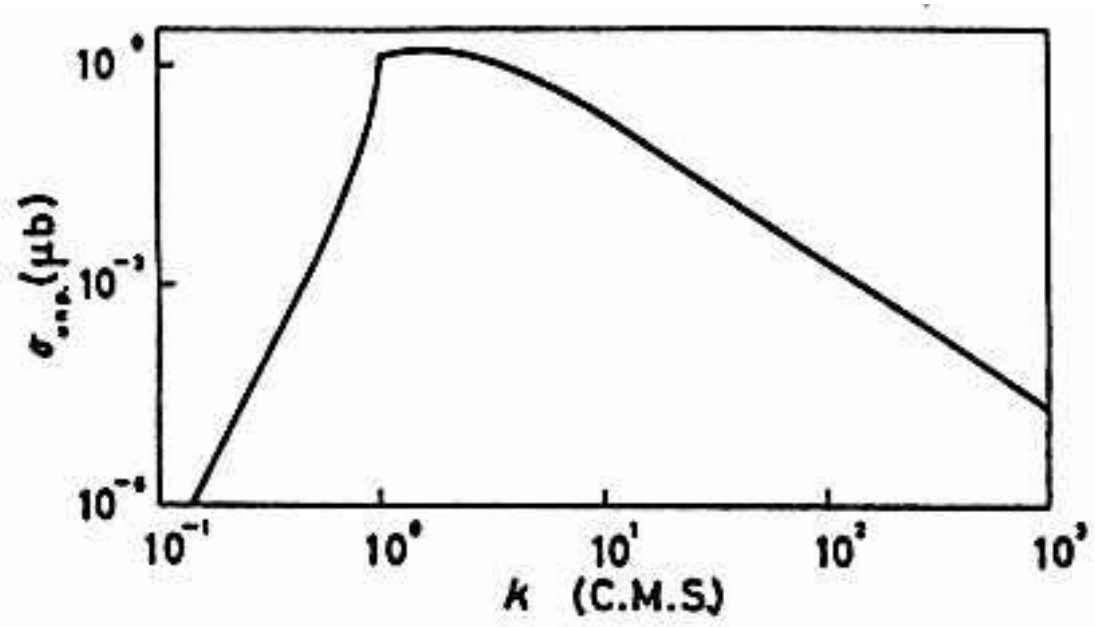

Figure 8. Total cross section of light-by-light scattering for unpolarized photons as a function of the energy k of each photon in the center-of-mass system, in units of mc^2.[63]

In the proposed second-round experiments, $\omega_1 = 4$ eV, while $\omega_2 = 37$ GeV, so that $k = 0.75$, and the light-by-light scattering cross section is about 2×10^{-32} cm^2. We suppose that for the light-by-light scattering experiment, the laser will have field-strength parameter $\eta = 0.8$, for which multiphoton effects become probable. According to charge-conjugation invariance (Furry's theorem), in the reaction

$$n\omega_1 + \omega_2 \rightarrow \omega_3 + \omega_4,$$

the number of laser photons n can only be odd. For the case of initial-state photons of definite helicity, there is an additional restriction that n be only 1 or 3.[64]† For the scattering of three 4-eV laser photons, we have $k = 0.75\sqrt{3} = 1.3$,‡ which is very close to the value at which the cross section for ordinary light-by-light scattering takes on its maximum.

---

† An oversimplified argument is that for forward scattering, $|J_z|$ must always be ≤ 2, while for $n > 3$ we would have $|J_z| > 2$ in the case of photons with definite helicity.

‡ In the case of a strong field it may be more proper to define $k \equiv (1/\overline{m})\sqrt{n\omega_1\omega_2} = (1/m)\sqrt{n\omega_1\omega_2/(1+\eta^2)}$, noting that $k = 1$ has the physical significance of being the threshold for pair creation. With $\eta = 0.8$, this would reduce our value of k to 1.0, with little effect on the light-by-light scattering cross section.

The cross section for the scattering of three laser photons against another photon has been recently derived by Affleck[64] in the limit $k \ll 1$:

$$\sigma_3 \sim 0.2\,\sigma_1 \eta^4 \left(\frac{\omega_1 \omega_2}{m^2}\right)^2 .$$

The η^4 dependence parallels the behavior in nonlinear Thomson scattering where the cross section for the absorption of n laser photons varied as η^{2n-2}. Near $k = 1$ we suppose the above expression is valid if we replace the low frequency estimate for σ_1 by the actual cross section shown in Figure 8. Then for ω_1 and ω_2 as stated above and $\eta = 0.8$ we estimate that $\sigma_3 \sim 7 \times 10^{-32}$ cm^2. This is about 3 times the cross section for the scattering of one laser photon! As for the Breit-Wheeler effect, the first observation of true light-by-light scattering will be in the presence of multiphoton nonlinearities.

Following the rate analysis given at the end of section 2-4b, a cross section of 10^{-30} cm^2 would yield one event in 10^6 pulses. We suppose that a factor of 10 improvement in the intensity of the backscattered photon beam would be made for the light-by-light scattering experiment. Also, a laser beam with $\eta = 0.8$ is 10 times as intense as that assumed in section 2-4b. If these factors are available, we would obtain one light-by-light scattering event per 150,000 pulses, which is not beyond experimental detection. The laboratory energies, ω_3 and ω_4, of the final-state photons are little different for the case of scattering of one or three laser photons, as $\omega_1 \ll \omega_2$. Indeed, our light-by-light scattering configuration is conceptually rather similar to the 'splitting' of a GeV photon in an external field.[65,66] The best signal for a light-by-light scattering event would be the detection of both photons ω_3 and ω_4 when the each has energy $\sim \omega_2/2$. In this case they emerge with laboratory angles $\sim m/\omega_2 \sim 10^{-5}$ rad. For this reason it is important that the angular divergence of the backscattered photon beam be small, as mentioned in section 2-4a.

Discussion of the experimental prospects for detection of light-by-light scattering date back to 1930,[67,68] in advance of theoretical considerations. The issue was reconsidered after the invention of the laser.[69–71] Experimental evidence for Delbrück scattering, and the splitting of a photon in the field of a nucleus is presented in ref. 72 and earlier references therein.

2-6. The Index of Refraction of a Strong Field.

In this section we discuss possible studies of the index of refraction induced by vacuum polarization in a strong wave field. The main effect accessible to the techniques of high-energy physics is vacuum Čerenkov radiation.[13]

Toll, in his Ph.D. dissertation,[73] was the first to calculate the index of refraction due to vacuum polarization. His results apply to a constant magnetic field, and to a constant field in which $E = B$ and $\mathbf{E} \cdot \mathbf{B} = 0$. As the frequency of a plane wave can be made arbitrarily small by a Lorentz transformation, the results should apply to this case also. Additional discussion of the index of a constant magnetic field is given in ref. 74. The index of refraction at frequency ω is found to be (for $B_{\text{eff}} \ll B_{\text{crit}} = m^2/e$)

$$n(\omega) = 1 + \frac{\alpha}{\pi}\left(\frac{B_{\text{eff}}}{B_{\text{crit}}}\right)^2 \left(N(\chi) + i\pi\frac{T(\chi)}{2\chi}\right),$$

where $N(\chi)$ and $T(\chi)$ are plotted in Figure 9, and

$$\chi = \frac{\omega}{m}\frac{B_{\text{eff}}}{m^2/e}.$$

For a constant magnetic field,

$$B_{\text{eff}} = \frac{1}{2}B\sin\phi.$$

where ϕ is the angle between $\mathbf{B}$ and the direction of propagation of the photon. For a plane wave,

$$B_{\text{eff}} = B\sin^2(\theta/2),$$

where θ is the angle between the directions of propagation of the plane wave and the photon.

For a plane wave the parameter χ is exactly the same as that introduced in section 2-4b when discussing the Breit-Wheeler effect:

$$\chi = \frac{\omega_\mu \omega'^\mu}{2m^2}\eta,$$

where ω' is the frequency and η the field-strength parameter of the strong plane wave. Note also that for a given field strength B, $n - 1$ is four times greater for a plane wave than for a constant magnetic field.

For $\chi \ll 1$ the function $N(\chi)$ takes on the value 14/45 for 'perpendicular' polarization, 8/45 for 'parallel' polarization, and 11/45 for either circular polarization

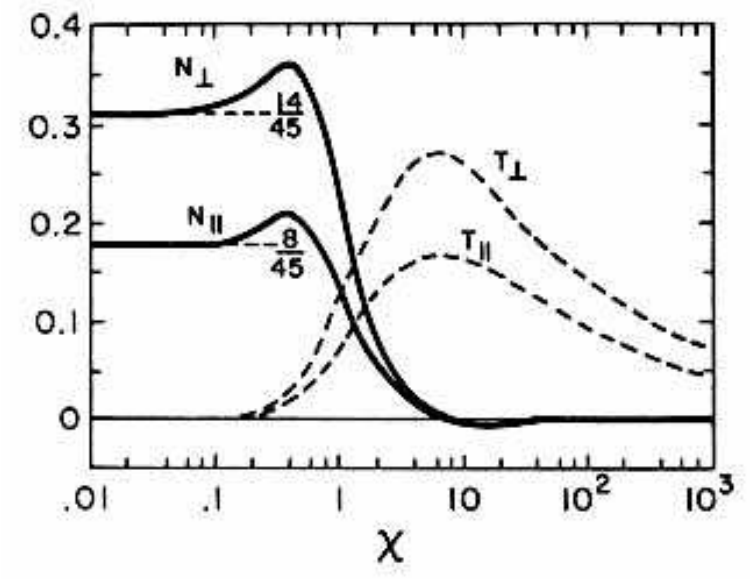

Figure 9. The functions $N(\chi)$ and $T(\chi)$ which appear in the real and imaginary parts of the index of refraction due to vacuum polarization effects in a strong field.[73]

of the photon. 'Parallel' polarization means the electric field vectors of the strong plane wave and the photon line up, *etc.* These limiting cases can be verified using the nonlinear Lagrangian of Euler and Heisenberg for constant fields[73,75] and for wave fields.[64]

> We will not be further concerned with the absorptive part, $T(\chi)$, which Toll related to the Breit-Wheeler pair-production process. Note that the function $N(\chi)$ drops (and becomes negative) when pair production can be caused by the probe photon ω. Toll's analysis (based on the static limit) ignores the possibility that several wave photons may be involved, which no doubt modifies the behavior of $N(\chi)$ and $T(\chi)$ when $\chi \gtrsim 1$ and $\eta \gtrsim 1$ also. Some consideration of this has been given by Becker and Mitter.[62]
>
> Toll[73] and others[74−78] have considered possible experimental effects of the index of refraction for optical photons in strong fields, but these are small and have never been observed. For example, the plane of polarization of an optical photon would be rotated about 10^{-12} radian per kilometer in a 40-kG magnetic field.[76]

Lutzky and Toll[79] remarked that the nonlinear index of refraction might lead to discontinuous behavior of propagating wavefronts, but did not suggest a specific experiment. Erber[13] has noted that the most accessible effect may be a sort of Čerenkov radiation of an electron in a strong field.

For a highly relativistic particle the Čerenkov threshold condition, $v = c/n$, becomes $2(n-1) = 1/\gamma_{\|}^2 = (1+\eta^2)/\gamma^2$. The factor $1+\eta^2$ arises because the particle has mass $\overline{m}$ in a strong field. For an electron colliding head-on with a circularly polarized plane wave of frequency ω and strength $\eta \gtrsim 1$, the threshold condition is

$$\gamma_{\min} = \left(\frac{mc^2}{\hbar\omega}\right)\sqrt{\frac{45\pi}{22\alpha}} \approx 10^7 \Rightarrow 5 \text{ TeV} \qquad \text{for} \qquad \hbar\omega = 1 \text{ eV},$$

noting that $B_{\text{eff}}/B_{\text{crit}} = \eta\hbar\omega/mc^2$.

The vacuum Čerenkov effect would appear as a correction to the nonlinear Compton scattering of the electron in such a strong field. A more complete analysis is needed to clarify its rôle among the higher-order effects of nonlinear quantum electrodynamics. When present, the Čerenkov radiation should be readily identifiable by its characteristic angular distribution. In addition, we anticipate that near the Čerenkov threshold there will be striking interference effects, such as those recently demonstrated between Čerenkov and synchrotron radiation for electrons in a polarizable medium with a weak applied magnetic field.[80]

Even when the strong wave field is probed by a high-energy photon, ω, there should be Čerenkov-like effects. The photon, and its surrounding cloud of vacuum polarization, propagates at velocity c/n, where $n(\omega)$ is the index as given above. If parameter $\chi \gtrsim 1$ for the high-energy photon in the strong wave field, the high-energy photon would have velocity greater than the phase velocity of lower-frequency photons, and its surrounding polarization pulse should be a source of Čerenkov radiation. This would be a correction to the already difficult light-by-light scattering experiment! For a 50-GeV photon moving opposite to an optical wave, the condition $\chi \sim 1$ requires wave-field strength $E \sim 4 \times 10^{12}$ V/cm.

Čerenkov-like radiation has been observed for optical photons in a dielectric medium.[81,82]

2-7. Unruh Radiation.

In this section we discuss a speculative effect which first aroused the proponents' interest in nonlinear electrodynamics. This example may serve to indicate the possibilities for phenomena beyond the more standard features to be reviewed in the preceding sections.

An appropriate point of departure is the work of Hawking[83] in which he associates a temperature with a black hole:

$$T = \frac{\hbar g}{2\pi c k}.$$

Here g is the acceleration due to gravity measured by an observer at rest with respect to the black hole, and k is Boltzmann's constant. The significance of this temperature is that the observer will find that (s)he is immersed in a bath of black-body radiation of characteristic temperature T. This is in some way due to the effect of the strong gravitational field on the ordinarily unobservable zero-point energy structure of the vacuum.

Contemporaneous with the work of Hawking several people considered quantum field theory according to accelerated observers. By the equivalence principle we might expect accelerated observers to experience much the same thermal bath as Hawking's observer at rest near a black hole. The efforts of Fulling,[84] Davies,[85] and Unruh[86] indicate that this may well be so. If a is the acceleration as measured in the instantaneous rest frame of an observer, then (s)he is surrounded by an apparent bath of radiation of temperature

$$T = \frac{\hbar a}{2\pi c k}.$$

Additional discussions of this claim are given by Sciama,[87] Sciama, Candelas and Deutsch,[88] and by Birrell and Davies.[89] 'Elementary' discussions are given by Boyer,[90] and by Donoghue and Holstein.[91]

Of experimental interest is the case when the observer is an electron. Then the electron can scatter off the bath of radiation producing photons which can be detected by inertial observers in the laboratory. This new form of radiation, which we will call *Unruh radiation*, is to be distinguished from the ordinary radiation of an accelerated electron. In particular, the intensity of radiation in the thermal bath varies as T^4. Hence we expect the intensity of the Unruh radiation to vary as $T^4 \sim a^4$. This result contrasts with the a^2 dependence of the intensity of Larmor radiation.

We illustrate this further with a semiclassical argument. The power of the Unruh radiation is given by

$$\frac{dU_{\rm Unruh}}{dt} = \text{energy flux of thermal radiation} \times \text{scattering cross section}.$$

For the scattering cross section we take

$$\sigma_{\rm Thomson} = \frac{8\pi}{3} r_o^2$$

where r_o is the classical electron radius. The energy density of thermal radiation is given by the usual Planck expression :

$$\frac{dU}{d\nu} = \frac{8\pi}{c^3} \frac{h\nu^3}{e^{h\nu/kT} - 1},$$

where ν is the frequency. The flux of the isotropic radiation on the electron is just c times the energy density. Note that these relations hold in the instantaneous rest frame of the electron. Then

$$\frac{dU_{\rm Unruh}}{dtd\nu} = \frac{8\pi}{c^2}\frac{h\nu^3}{e^{h\nu/kT}-1}\frac{8\pi}{3}r_o^2.$$

On integrating over ν we find

$$\frac{dU_{\rm Unruh}}{dt} = \frac{8\pi^3\hbar r_o^2}{45c^2}\left(\frac{kT}{\hbar}\right)^4 = \frac{\hbar r_o^2 a^4}{90\pi c^6},$$

using the Hawking-Davies relation $kT = \hbar a/2\pi c$.

A variation of the preceding argument has been given by Gerlach.[92] Again the key idea, taken as an assumption, is that an accelerated observer can have a non-trivial interaction with the vacuum fluctuations of the electromagnetic field. We suppose that these fluctuations, $\Delta\mathbf{E}$, lead to an additional acceleration of the observer, which for an electron yields $\langle\Delta a^2\rangle = e^2\langle\Delta\mathbf{E}^2\rangle/m^2$. The apparent strength of the vacuum fluctuations depends on the acceleration of the electron, Planck's constant, and the speed of light, but not the external electric field. By dimensional arguments, $\langle\Delta\mathbf{E}^2\rangle \sim \hbar a^4/c^7$. The Unruh radiation rate can now be estimated from the Larmor formula by inserting the fluctuation acceleration:

$$\frac{dU_{\rm Unruh}}{dt} = \frac{2}{3}\frac{e^2\langle\Delta a^2\rangle}{c^3} \sim \frac{\hbar r_o^2 a^4}{c^6}.$$

A numerical comparison with Larmor radiation is instructive:

$$\frac{dU_{\rm Unruh}}{dt} \sim 4.1\times10^{-118}a^4 \qquad \text{(in c.g.s. units)}$$
$$\frac{dU_{\rm Larmor}}{dt} \sim 5.7\times10^{-51}a^2.$$

The two radiation effects are comparable for $a \sim 3\times10^{33}$ cm/sec^2 $\sim 3\times10^{30}g$, where g is the acceleration due to gravity at the surface of the earth. If this acceleration is to be provided by an electric field we then need

$$E \sim 2\times10^{18} \text{ volts/cm}.$$

This is about two orders of magnitude larger than the 'critical' field $m^2c^3/e\hbar$ introduced in section 1. The consequence is that the Unruh radiation effect will manifest

itself only in the context of the other nonlinear electrodynamic phenomena discussed in the preceding sections. Untangling the various features of radiation when $E > 10^{18}$ volts/cm will be a formidable challenge. For example, the field-strength required for significant Unruh radiation is similar to that for vacuum Čerenkov radiation. In addition, Unruh radiation will include e^+e^- pairs as well as photons.

Note that $E_{\rm lab}$ need not be $\sim 3 \times 10^{18}$ volts/cm if a relativistic electron probes the field. For a 50-GeV electron $\gamma \sim 10^5$ so that $E_{\rm lab} \sim 3 \times 10^{12}$ volts/cm will suffice. This is only about 30 times stronger than the electric field of the second-round laser discussed insection 2-4a.

If we divide the expression for the rate of Unruh radiation by the incident photon energy flux we obtain the cross section:

$$\sigma_{\rm Unruh} \sim \alpha \, \sigma_{\rm Thomson} \left(\frac{E}{m^2/e} \right)^2 .$$

This might correspond to the Feynman diagram sketched below, in which a virtual electron-positron pair created in the strong laser field (rather than in the electron's own field or that of another charge) emits a photon which scatters off the electron. Similar diagrams appear in discussions of vacuum polarization effects near nuclei, where the coupling, $\times$, to the external potential leads to the Lamb shift at low energies, while for energies $\gtrsim m$, the coupling is dominated by a single virtual photon tied to the nucleus. In the case of Unruh radiation, energies $\sim m$ are achieved via the coupling of the virtual pair to large numbers of photons in the strong background field, which leads to new phenomena in the semiclassical limit.

The semiclassical analysis presented here bears some relation to the method of virtual quanta.[46] In the latter, an electrostatic field of limited extent appears as a pulse of radiation to a moving observer. That pulse is then resolved into its fourier components–the virtual photons. For the Hawking-Unruh effect, it may be argued that the vacuum fluctuations of the eletromagnetic field, ordinarily unobservable, take on the character of a thermal spectrum according to an accelerated observer. Of course the full justification of this point of view should be

agreement with the results of a complete QED analysis, presently unavailable. A step in this direction is the dissertation of Myhrvold,[93] but the form of his argument does not shed immediate light on experimental considerations. See also an interesting paper by Ritus.[94]

Bell and Leinaas[95] have suggested that the inability of synchrotron radiation to fully polarize a circulating electron beam[96] is due to the thermalizing influence of the Hawking-Unruh radiation bath seen by an accelerating electron. Salam and Strathdee,[97] Barshay and Troost,[98] and Hosoya[99] have considered the possible relevance of the Hawking-Unruh temperature to thermodynamic models of the strong interaction.

2-8. Photoproduction of W Bosons.

In this section we consider the possibility of studying the reaction

$$\gamma e \to W\nu$$

by creating a backscattered photon beam at the SLC intersect.

When sufficient energy becomes available, W bosons can be produced in large quantities at e^+e^- colliders via the reaction

$$e^+e^- \to W^+W^-.$$

Apart from the study of the decay of the W boson, there is intrinsic interest in this reaction as the first test of the couplings among the gauge bosons themselves, at the γWW and Z^0WW vertices. Of particular interest is the γWW coupling, which depends on the magnetic moment of the W, predicted to be e/M_W in the standard model.[100] This is often written

$$\mu_W = \frac{e}{2M_W}(1+\kappa),$$

where κ is called the anomalous magnetic moment of the W. The standard model prediction is then $\kappa = 1$. The total cross section for $e^+e^- \to WW$ turns out to be quite sensitve to the value of κ, leading to an important experimental test of the standard model.[101,102]

The coupling of photons to massive vector mesons was first considered by Feynman,[103] who tacitly assumed $\kappa = 0$. Lee and Yang[104] and Lee[105] noted that a necessary (but not sufficient) condition for a renormalizable theory of massive

vector mesons is that the anomalous magnetic moment, κ, be 1. Bardeen *et al.*[100] confirmed this to be the case in the Weinberg-Salam model. A brief argument is that the photon is a component of the W^0 member of the weak-isospin triplet ($W^+,\ W^0,\ W^-$), so the requirement of weak-isospin symmetry at the γWW vertex adds a piece to the vertex factor, which corresponds to $\kappa = 1$.

The magnetic structure of the W boson can be probed at lower laboratory energies in the reaction $\gamma e \to W\nu$, as noted by Mikaelian.[14,15] This proceeds via the two diagrams shown in Figure 10. The second diagram, which does not involve a γWW vertex, will not contribute if the incident photon has right-hand circular polarization. (Angular momentum cannot be conserved, noting that only left-handed electrons interact weakly.) The cross section for this reaction is not large, varying as

$$\sigma_{\gamma_R e_L \to W\nu} \sim 94\left(1 - M_W^2/s\right)^2 \text{ pb}$$

near threshold. Figure 11 sketches the energy dependence of the cross section as calculated in detail.[16]

Near threshold the cross section varies as $8\sqrt{2}\,\alpha G_F\,\mathbf{p}_\nu^2/s$. One power of $\mathbf{p}_\nu$ comes from phase space, and the other from the square of the $V - A$ matrix element. At high energies the cross section approaches the constant value $2\sqrt{2}\,\alpha G_F = 94$ pb.

If a backscattered photon beam is obtained from the collision of 50-GeV electrons with a 0.308-μm laser beam, the peak photon energy is 37 GeV (Figure 2). When this beam is in collision with another 50-GeV electron (or positron) beam, $\sqrt{s} = 87$ GeV, at which the total cross section is 0.5 pb. If 60-GeV electron beams were available, we could have $\sqrt{s} = 107$ GeV, for which the cross section is 7.5 pb. A laser beam of sufficient intensity and duration to scatter 100% of the electrons would intercept the beam a few millimeters from the nominal e^+e^- interaction point. There would be no need to deflect an unscattered remnant of the original electron beam. The effective $e\gamma$ luminosity (for W production) might be 5% of the e^+e^- luminosity, say 5×10^{29} cm^{-2}s^{-1}. A major run of 100 days with 60-GeV polarized electrons would then yield about 30 events. An earlier discussion of such possiblities has been given by Akerlof.[106]

The angular distribution of the W boson is quite sensitive to its anomalous magnetic moment, κ.[14] This is sketched in Figure 12, for center-of-mass energies corresponding to 50 and 60-GeV electron beams. A very strong forward-backward asymmetry is predicted in the standard model compared to the case of no anomalous

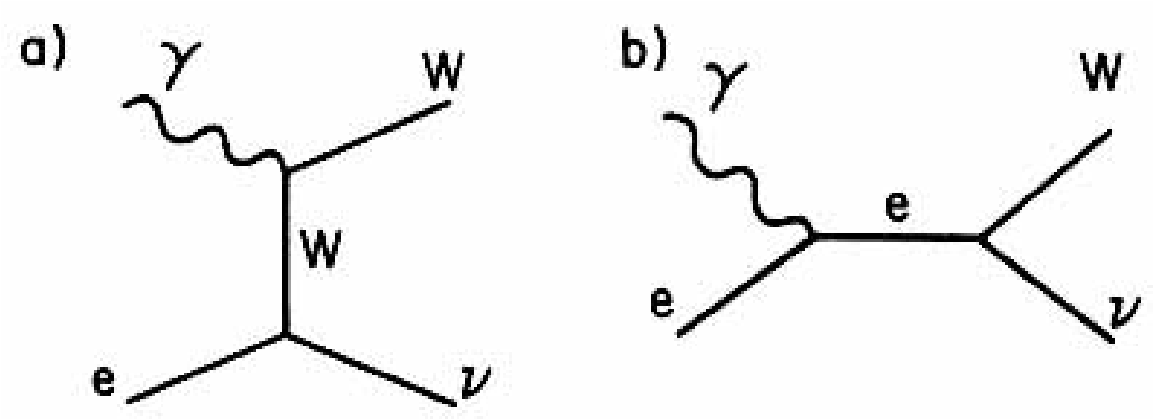

Figure 10. The two Feynman diagrams which contribute to the reaction $\gamma e \to W\nu$. Diagram **b)** can be suppressed by the use of right-hand circularly polarized photons.

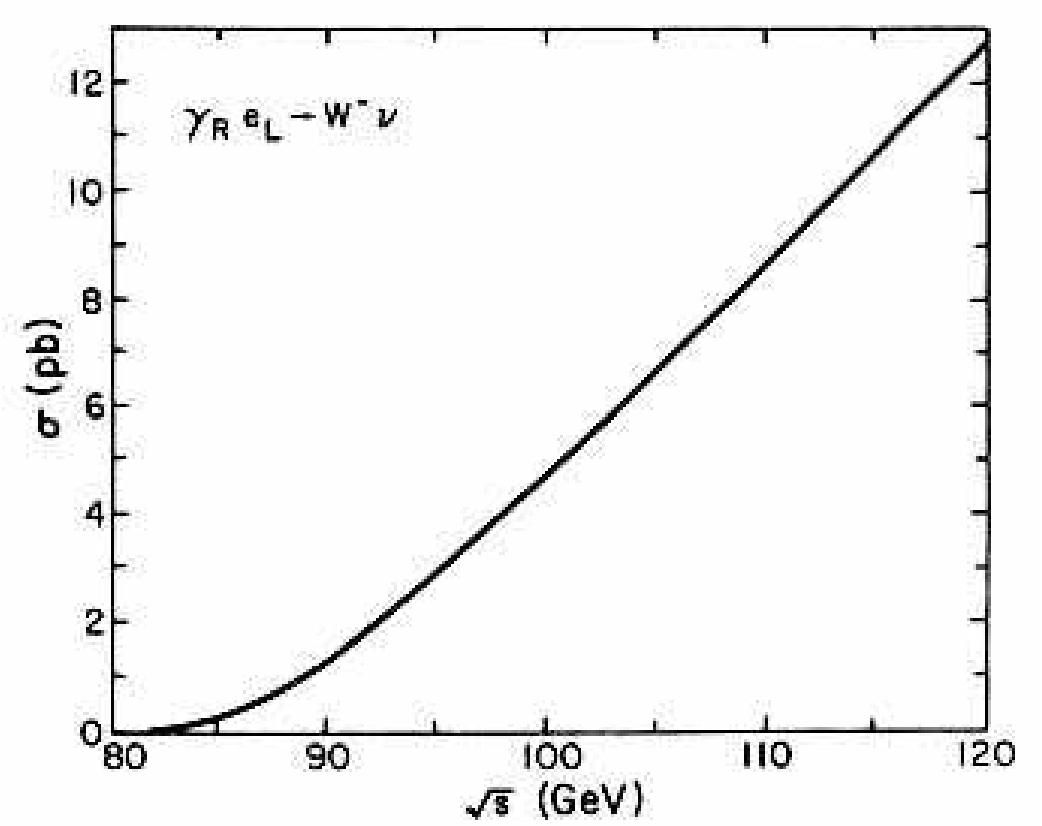

Figure 11. The dependence on center-of-mass energy of the total cross section for the reaction $\gamma_R e_L \to W\nu$.[16]

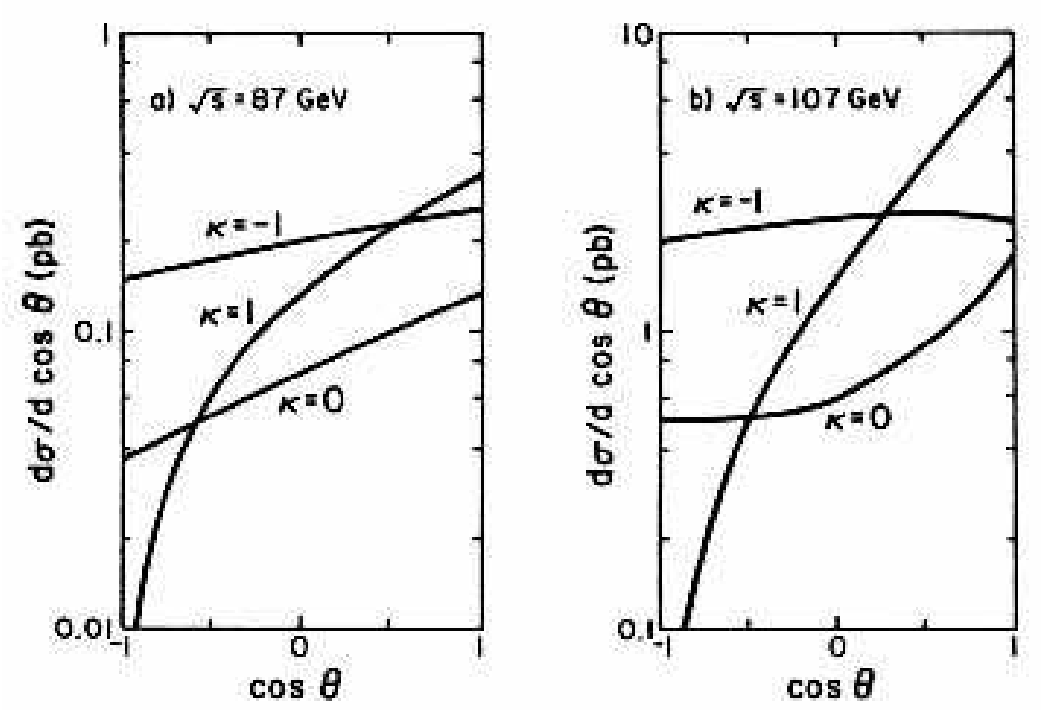

Figure 12. The angular distribution of the W boson produced in the reaction $\gamma e \to W\nu$.[14] Angle θ is measured between the photon and the W boson in the center-of-mass frame. The center-of-mass energies correspond to those obtained from **a)** 50, and **b)** 60-GeV electron beams, one of which is backscattered off a laser beam of 0.308 μm wavelength.

magnetic moment, which should be testable with a small number of events.

Technically it would be easier to arrange for the reaction $\gamma e \to W\nu$ via virtual photons in the reaction $e^+e^- \to eW\nu$.[14,16,107–111] A detailed study is required to determine whether the luminosity is greater for real or virtual photons. However, unless the spectator electron is detected, no asymmetry in the angular distribution would be observed for the e^+e^- reaction, and the dependence on the size of the anomalous moment would be much less clear. The spectator electron would emerge with about 13 GeV, at an angle $\sim 10^{-5}$ rad to the electron beam. Further study is needed to decide whether this electron could be identified against the background of off-beam-energy electrons due to beamstrahlung.

3. The Nonlinear Thomson Scattering Experiment.

In this section we present details of the proposed experiment to study the nonlinear Compton effect. A laser beam of 1.05-μm wavelength and peak field strength parameter $\eta = eE/m\omega c = 0.4$ will be brought into collision with 25-MeV electrons in the apparatus sketched in Figure 13. In the rest frame of the incident electron, the laser photons have energy about 115 eV, so the electron recoil will be negligible, and the process to be studied is nonlinear Thomson scattering rather than Compton scattering. The theoretical understanding of both processes has been reviewed in sections 2-2 and 2-3.

In practice it may be preferable to use a laser of 10-μm wavelength, which is needed for other aspects of the experimental program at the Brookhaven Accelerator Test Facility. Section 3 of the present proposal records how the option to use a 1-μm wavelength is also very viable.

The 25-MeV electron beam will be produced by the Accelerator Test Facility (ATF), whose rather small emittance, $3(\pi) \times 10^{-10}$ rad-m (at 25 MeV), permits the electron beam to be focused to a spot of radius 1 μm with a depth of focus $\beta^\star = 1.6$ mm.† The laser beam is brought into head-on collision with the electrons by an off-axis parabolic mirror with $f/d = 3$. A hole of 300-μm diameter in the mirror lets the electron beam and the backscattered photons pass through. The unscattered laser beam will be collected in a second mirror and reflected out of the electrons' path into a beam-flux monitor. The electrons are deflected by 23° in a dipole magnet 0.5 m downstream of the collision point, and their momentum spectrum recorded by the CCD array. Photons which are backscattered to within 10 mrad of the electron-beam direction are analyzed in an x-ray spectrometer located 1 m downstream of the collision point.

For an estimate of the scattering rate, we suppose both the electron bunch and the laser pulse have FWHM of 2 ps. The laser beam has total energy of 0.1 Joule. The electron beam is taken to have a Gaussian radial profile, while the laser beam has the spatial dependence of a (diffraction-limited) Gaussian beam modulated by a sech^2 (soliton) pulse shape:[112]

$$I_{\rm laser}(r,z,t) = \frac{I_{\rm max}}{1+z^2/{z_o}^2}\exp\left(-\frac{r^2}{2\sigma^2(z)}\right)\mathrm{sech}^2\left(\frac{t-z/c}{\tau}\right).$$

† The depth of focus is the distance from the focal plane at which the spot size has grown by a factor of 2 in area. In accelerator argot, this is called the $\beta^\star$, while in laser lingo it is called the confocal parameter or, sometimes, the Rayleigh range.

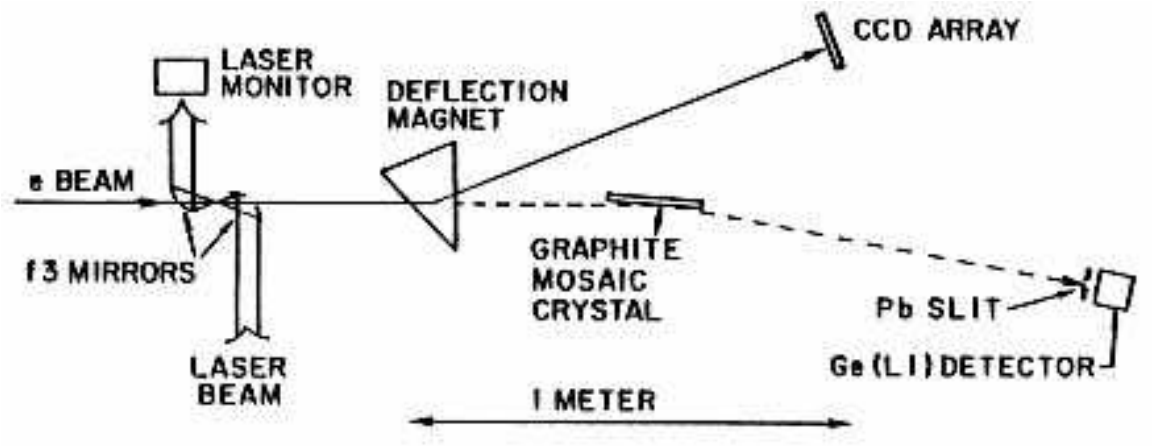

Figure 13. Layout of the proposed experiment.

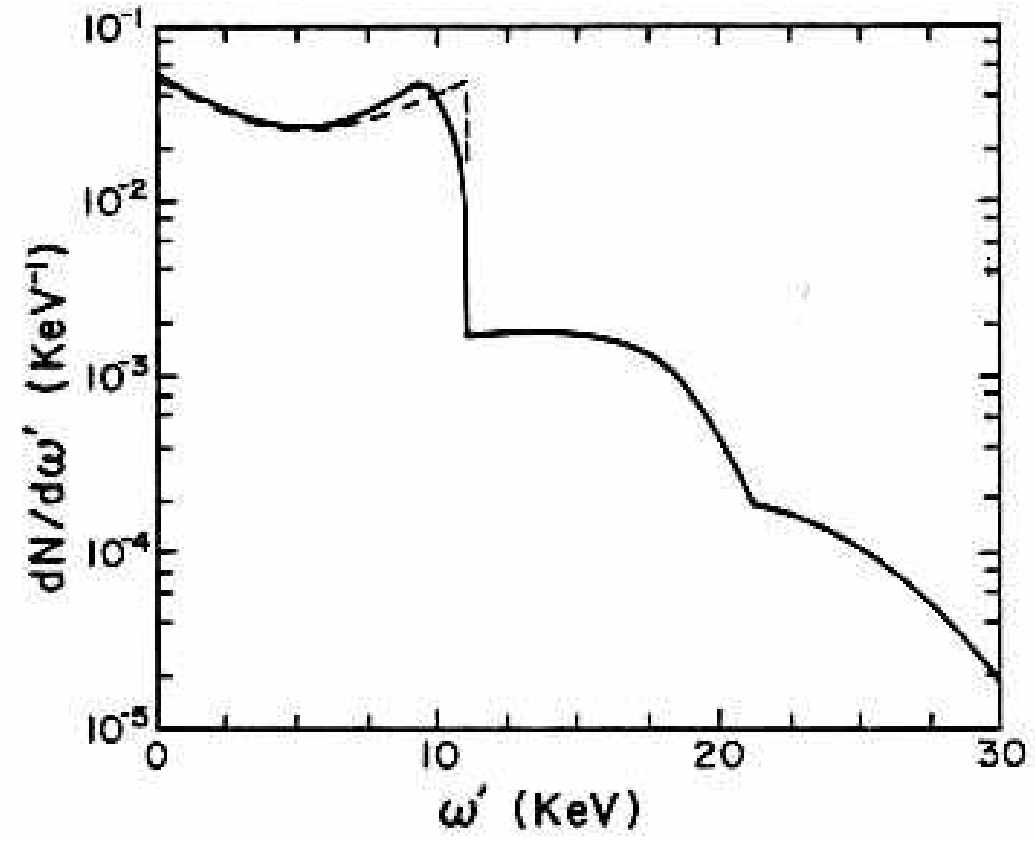

Figure 14. The scattering rate for a single 25-Mev electron in head-on collision with a laser beam of wavelength 1.05 μm. The laser pulse has 0.1-Joule energy and 2-ps pulse length, and is focused in an $f3$ mirror to achieve peak field-intensity parameter $\eta = 0.4$ The total scattering rate is 0.4 per electron. The dashed curve is the rate for Compton scattering if nonlinear effects are ignored.

In this, the variance of the spot size, $\sigma(z)$, grows as $\sigma_o\sqrt{1+z^2/{z_o}^2}$, where z_o is the confocal parameter. For a diffraction-limited beam optimally filling the mirror aperture, $\sigma_o = 0.43\lambda f/d$, and $z_o = 2.28\lambda(f/d)^2$. In the present case, $\sigma_o = 1.4$ μm, and $z_o = 22$ μm. For a laser pulse of 2 ps FWHM, the parameter τ is 1.14 ps. The above variation of electron and photon flux over the interaction volume is then combined with the cross section as stated in section 2-3 to give the scattering rate.

Figure 14 summarizes the spectrum of scattered photons. The total scattering rate is 0.4 per beam electron. Thus the probability that an electron scatters twice while crossing the laser beam is 0.16. This places an important constraint on the x-ray detector, which must be able to tell a double scatter at the first harmonic from the rarer case of a single scatter at the second harmonic. The detector will not be able to resolve multiple photons in time during the 2-ps pulse, but must deflect x-rays of different energies by different angles, so they can be separately counted. This is provided by a detector based on Bragg scattering off a graphite crystal at near-grazing incidence. Such devices have limited utility for x-ray energies above 30 keV. To be sensitive up to third harmonic scattering we desire the fundamental to be at about 10 keV, which leads to the choice of a 25-MeV electron beam, when using a laser wavelength of 1.05 μm.

In the following subsections we discuss briefly the electron beam (3-1), the laser focus (3-2), the laser system itself is discussed in section 4), the spectrometer to monitor the electron beam (3-3), the x-ray spectrometer (3-4), backgrounds (3-5), and the scenario for data collection (3-6). The possibility of coherent scattering of laser light off a bunched electron beam is considered in section 3-7, but will not be practical for the proposed experimental configuration.

3-1. The Electron Beam.

Some basic parameters of the proposed Accelerator Test Facility are summarized in Table 1.[113] The original proposal called for a single accelerating section powered by a 36-MW klystron. It now appears that the available klystron will be rated to closer to 30 MW, so the nominal beam energy would be closer to 40 MeV. If a second accelerator section and klystron are added, 80-MeV beams would also be available.

The geometric emittance of 1.5×10^{-10} rad-m holds at 50 MeV, and varies linearly with beam energy. For the present experiment we wish a 25-MeV beam, so the geometric emittance would be 3×10^{-10} rad-m. These very low emittances are achieved with a very small illumination (20-μm radius) at the photocathode of

Table 1. Accelerator Test Facility Specifications

Parameter	ATF Proposal	Present Proposal
Photocathode gun voltage	400 kV	400 kV
Photocathode gun pulse length (FWHM)	6 ps	2 ps
Photocathode laser wavelength	0.532 μm	0.525 μm
Cathode radius	20 μm	20 μm
Transverse energy at cathode	~ 0.1 eV	~ 0.1 eV
Invariant emittance out of gun ϵ_n	1.35×10^{-8} mc-m	1.35×10^{-8} mc-m
Cathode current density	200 A/cm^2	200 A/cm^2
Electrons per bunch	$\sim 10^5$	$\sim 10^5$
Beam energy	50 MeV	25 MeV
Klystron peak power	36 MW	9 MW
Klystron repetition rate	≤ 180 pps	$\leq$ 180pps
Electron energy spread $\Delta E/E$ (FWHM)	$\leq 1\%$	$\sim 0.1\%$
Geometric transverse emittance at experiment	1.5×10^{-10} rad-m	3×10^{-10} rad-m

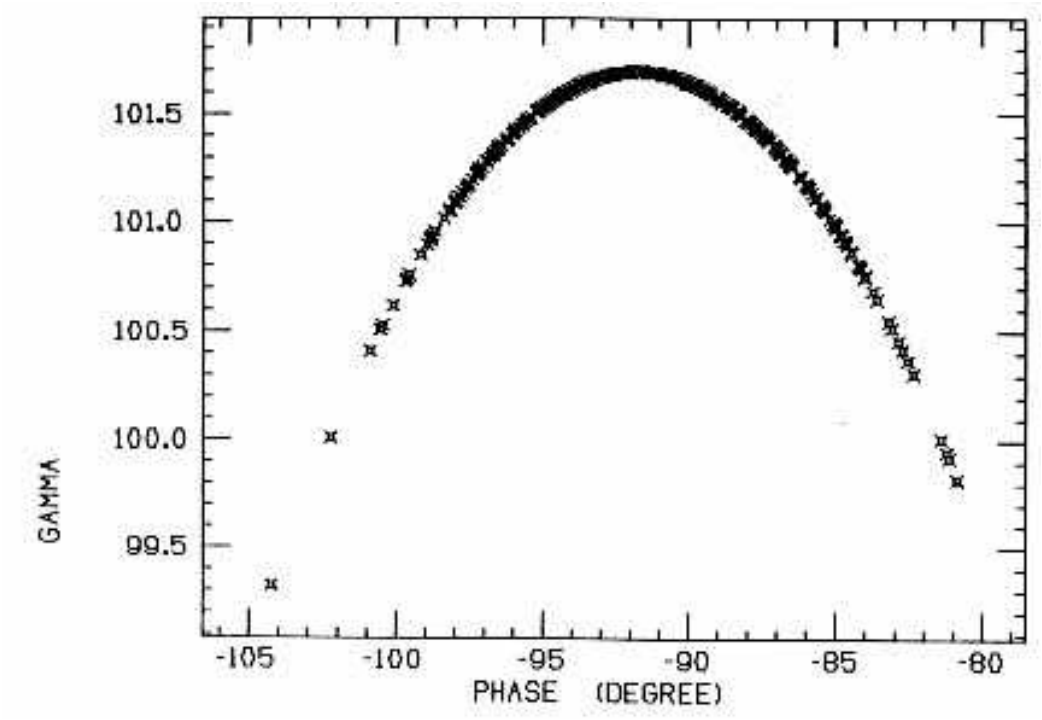

Figure 15. Electron-beam energy, $E = \gamma mc^2$, as a function of the rf phase, for 50-MeV nominal beam energy.

the electron gun, and with a very small transverse energy (0.1 eV) of the electrons ejected from the cesium-antimony photocathode.[114]

Figure 15 illustrates how the accelerated electron energy, $E = \gamma mc^2$, varies with the phase of the electron relative to the 2856-MHz accelerating field. At this frequency 1° of phase equals 0.97 ps in time. The stated electron-energy spread of $\Delta E/E = 1\%$ derives from an assumption of a 6-ps bunch length with ±5 ps jitter with respect to an rf cycle. For the present experiment we plan to use a narrower electron bunch, 2-ps long, synchronized to the rf to 1-ps accuracy, as described in section 4. Assuming the electrons' paths through the gun are isochronous to the needed accuracy, an energy spread of $\Delta E/E = 0.1\%$ should be achieved.

The electron beam is brought from the linac to the experiment in a beam transport which permits a final focus of 1-μm radius. The corresponding beam divergence is 3×10^{-4} radians, and the depth of focus is $\beta^\star = 1.6$ mm. Emittance-defining collimators along the beam transport will permit cleanup of tails and further reduction of the emittance, if desired.

If a momentum-analysis section is included in the beam transport, the beam-energy spread could be collimated to 0.01%, with a loss in beam intensity. Such a narrow energy spread could be useful in conjunction with the excellent resolution of the analysis spectrometer discussed in section 3-3.

The linac structure and any collimators in the beam transport are a likely a source of x-rays, which will be the principal source of background for the experiment. This background would be greatly reduced by a bend in the beamline, as would be provided by a momentum-analysis section.

3-2. The Interaction Region.

The laser beam is brought to a focus in a head-on collision at the final focus of the electron beam. The power level of the laser beam is 100 GW, which requires the use of reflection optics. An off-axis parabolic mirror of $f/d = 3$ focal length/aperture will focus the laser beam. The mirror radius will be 1 cm, sufficient to intercept the growth of the laser beam between the laser and the mirror. Hence the mirror will be located 6 cm from the e-laser interaction point. At this distance the electron beam radius is 18 μm r.m.s. The electron beam will pass through a 300-μm-diameter hole in the mirror, as sketched in Figure 13.

The unscattered laser beam will be collected in a second parabolic mirror, and brought to a beam-flux monitor. To aid in alignment of the mirrors with respect to the electron beam a quadrant detector will be located on the upstream face of the

second mirror. The two mirrors will be mounted together on an x-y-z translation stage capable of 0.1-μm steps, such as manufactured by Klinger.

The interaction region will be maintained at a vacuum of 10^{-5}-10^{-6} torr. The drive motors for the translation stage could be located inside the vacuum chamber while maintaining a vacuum of 10^{-6} torr. The vacuum chamber will be constructed to be interchangeable with that for the laser-grating experiments at the Accelerator Test Facility.

3-3. The Electron Spectrometer.

After the electron beam passes the interaction point, it must be deflected to one side to allow the scattered photons to be analyzed. The magnet required for this also serves as the dispersive element in a precision electron spectrometer, sketched in Figure 13. The dipole magnet has a field of 880 Gauss, a field integral of 0.033 Tesla-m (for the 25-MeV beam), and deflects the electrons by 23°. The electron beam then impinges on a CCD array with 385 × 580 pixels each 25-μm square, located 1 m downstream of the deflection magnet. The spectrometer will be capable of 1-keV resolution for the 25-MeV electrons.

The spectrometer will serve as the primary electron-beam-flux monitor, measuring the beam intensity as a function of momentum. An additional rôle is possible if the momentum-analysis segment of the electron beam line is constructed. In that case the beam could be stopped down to a 0.01% momentum bite, corresponding to an energy width of 2.5 keV. Then electrons which scatter a laser photon to produce an x-ray of 10 keV or more could be distinguished from the unscattered electrons in the electron spectrometer.

The electron spectrometer will be in a different configuration from that used in the laser-grating experiment,[4] with the magnet now immediately after the interaction region to improve the acceptance of the x-ray spectrometer. The quadrupole triplet, which provides a line focus on the CCD array for the laser-grating experiment, will not be needed. Only about 50 columns of the CCD array will be populated with electrons in the present experiment. If the readout is restricted to these columns the readout dead-time would be reduced by a factor of 8, permitting data collection at about 10 pps.

3-4. The X-Ray Spectrometer.

As shown in Figure 14, laser photons that backscatter off the electron beam are Doppler-shifted to x-ray energies. During a 2-ps pulse of 10^5 electrons we expect

4×10^4 x-rays to be produced. To analyze this we need an x-ray spectrometer which disperses x-rays of different energies to different positions. Then a total absorption detector which counts the number of x-rays at a fixed position will determine the x-ray flux within a well-defined energy bin.

The nonlinear mass-shift effect (at the proposed laser intensity) reduces the endpoint of the x-ray spectrum by some 15% compared to weak-field Compton scattering. (See Figure 14.) Thus bins of 1% in x-ray energy would be quite suitable to analyze the effect. This is 10–100 times broader than the bandwidth of a typical x-ray monochromator which uses a perfect crystal. However, our requirements are well matched to the capability of a spectrometer based on a flat pyrolitic graphite crystal,[115] in which there is a spread (or mosaic) of 0.8° in the orientations of the planes of the microcrystals.

The simultaneous functioning of the graphite crystal as a dispersive and focusing element is sketched in Figures 16 and 17. We are fortunate in having a very good approximation to a point source at the electron-photon interaction region. This is shown at distance L from the center of the crystal, which is oriented at the Bragg angle θ_B for x-rays of energy E. An x-ray of energy E traveling along the central ray will penetrate into the crystal until it meets a microcrystal with its crystal planes at angle θ_B to the x-ray. The x-ray then scatters by angle $2\theta_B$ with about 40% efficiency.

Now consider an x-ray also of energy E, but which makes angle $\Delta/2$ to the central ray, as shown in Figure 16. If the graphite were in the form of a single perfect crystal, this x-ray would not strike the crystal planes at the Bragg angle θ_B, and would not be scattered. But if Δ is less than or equal to the mosaic spread of the graphite crystal then the x-ray does scatter off some microcrystal, again with scattering angle $2\theta_B$. The paths of the two scattered x-rays cross approximately at distance L from the crystal. That is, the variable orientation of the microcrystals within the flat macroscrystal duplicates the focusing effect (in the scattering plane only) of a bent perfect crystal.

Next consider the case of x-rays with energy $E + \delta E$, as shown in Figure 17. The corresponding Bragg angle is now $\theta_B - \delta\theta_B$. Such an x-ray traveling along the central ray at angle θ_B to the crystal could not scatter off a perfect crystal. But if $\delta\theta_B < \Delta/2$, the x-ray will find some microsrystal off which it can scatter, with scattering angle $2(\theta_B - \delta\theta_B)$. Similarly, x-rays of energy $E + \delta E$ which make small angles to the central ray also scatter off some microsrystal, and are brought to a focus at distance L from the crystal. Because of the dependence of the Bragg angle

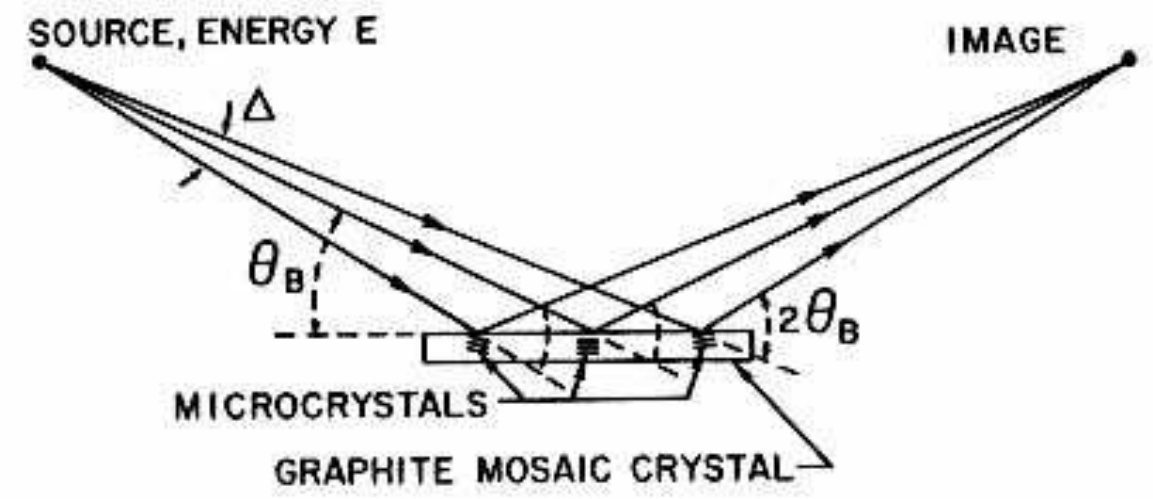

Figure 16. The scattering of monoenergetic x-rays by a graphite mosaic crystal. The scattering angle is always twice the Bragg angle θ_B. The mosaic spread, Δ, of orientations of the microcrystals results in a focusing geometry with angular acceptance Δ.

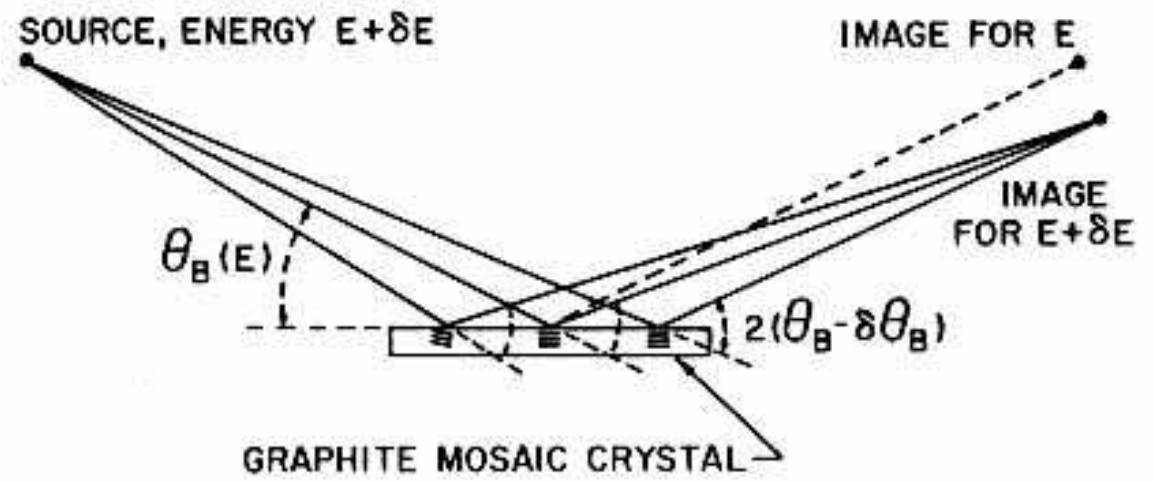

Figure 17. X-rays of energy $E + \delta E$ are focused by Bragg reflection off a graphite mosaic crystal to a different point than those of energy E.

on x-ray energy, the scattered x-rays disperse along a focal plane as desired.

For numerical computation it is useful to note the Bragg relation for graphite:

$$\sin\theta_B = \frac{1.85}{E[\text{keV}]}.$$

This follows from the usual form of Bragg's law,

$$\sin\theta_B = \frac{\lambda}{2d},$$

the useful conversion formula

$$\lambda[\text{Å}] = \frac{12.38}{E[\text{keV}]},$$

and the fact that the crystal-plane separation in graphite is $2d = 6.71$ Å. The dispersive effect can be calculated by taking the derivative of the Bragg law:

$$\cot\theta_B\,\delta\theta_B = \frac{\delta E}{E},$$

which is well aproximated in graphite for $E \gtrsim 10$ keV by

$$\delta\theta_B = \frac{1.85}{E[\text{keV}]}\frac{\delta E}{E}.$$

For example, with $E = 10$ keV, the Bragg angle is 186 mrad, so the scattering angle is 372 mrad. For a 1% bite $\delta E/E$ about 10 keV, the angular bite is $\delta\theta_B = 1.86$ mrad. If the distance L from the source to the crystal, and hence from crystal to the detector, is 1 m, then a slit of 3.7 mm at the face of the detector would define the 1% energy acceptance.

The angular acceptance (in the scattering plane) of the spectrometer is in prinicple limited only by the mosaic spread angle $\Delta = 0.8^\circ = 14$ mrad. To take full advantage of this range the crystal must have length

$$l = \frac{L\cdot\Delta}{\sin\theta_B} = \frac{L\cdot\Delta\cdot E[\text{keV}]}{1.85}.$$

We wish to analyze the third harmonic scattering, for which $E \sim 30$ keV, so this requires crystal length $l \sim 23$ cm.

The flat-crystal geometry of the spectrometer does not provide any focusing transverse to the scattering plane. With source and detector equidistant from the crystal, the transverse size of the image is twice that of the intercept of the x-rays

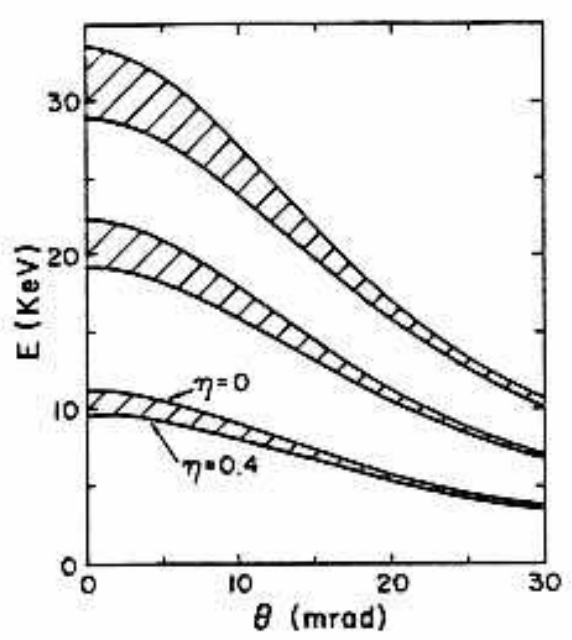

Figure 18. The relation between x-ray energy and production angle for the first three harmonics in nonlinear Thomson scattering of 25-MeV electrons and a 1.05-μm laser beam. The bands are due to the intensity dependence of the nonlinear effects.

at the crystal. With a Ge(Li) detector of 50-mm diameter, the useful width of the graphite crystal is then 25 mm. Hence there will be acceptance for x-rays which make angle θ of up to 12.5 mrad with respect to the direction of the electron beam. As just noted, there cannot be full angular acceptance for angles $\theta > \Delta/2 = 7$ mrad.

There is an additional effect on the transverse size of the image on the detector. Due to the mosaic spread, Δ, of the microcrystals, the x-rays of a given energy which scatter from a given point on the graphite crystal have a spread of angles, Δ, in azimuth. The x-rays scatter at polar angle 2θ and describe an arc of length $l = L \cdot \Delta \cdot \sin\theta$ over the face of the detector. For $L = 1$ m, $\Delta = 14$ mrad, and $\theta_B = .186$ corresponding to 10 keV, we have arc length $l = 5$ mm.

In summary, the configuration of the x-ray spectrometer is simple and classic. The graphite crystal is mounted on a rotating stage located 1 m from the e-laser interaction point, along the line of the electron beam (see Figure 13). X-rays of a given energy are brought to a focus 1 m from the crystal, after scattering at twice the Bragg angle. A slit defines the width of the energy bin, and the number of x-rays in that bin is determined by measurement of the sum of their energies in a Ge(Li) solid state detector, such as Ortec Model GLP-50/10.

Figure 18 shows the relation between x-ray energy and angle θ relative to the direction of the electron beam for the first three harmonics in nonlinear Thomson scattering. Because the electron beam will pass through regions of various laser-beam intensity, there is a range of x-ray energies produced at any fixed angle. The bands in Figure 18 show this range corresponding to field-strength parameter η between 0 and 0.4. The scattering rate will be much higher on the $\eta = 0.4$ edge of the bands. With a graphite crystal of mosaic spread angle $\Delta = 14$ mrad, there will be full collection efficiency out to production angle 7 mrad. The collection efficiency at larger angles will be determined experimentally by a calibration run with reduced laser intensity, so that $\eta \sim 0$ and we may utilize the well-known spectrum of x-rays from linear Thomson scattering.

3-5. Backgrounds.

Background x-rays could arise from synchrotron radiation in the dump magnet (or beam-momentum-selection magnets if present), from bremsstrahlung of the electron beam off residual gas in the vacuum chamber, or from bremsstrahlung off the emittance-defining collimators in the beam line. The latter effect is likely to be the most serious, but is hard to estimate quantitatively. Considerable care will be required to install the necessary shielding against this source. We now show that the other two sources may be calculated to be negligible.

Concerning synchrotron radiation, recall that the characteristic frequency radiated by an electron of energy $E = \gamma mc^2$ in a magnetic field B is

$$\omega \sim \gamma^3 \omega_o = \gamma^2 \frac{eB}{mc} = 511\gamma^2 \frac{B}{B_{\rm cr}}[\text{keV}],$$

where $B_{\rm cr} = m^2c^3/e\hbar = 4.41 \times 10^{13}$ Gauss. Thus for $E = 25$ MeV and $B = 880$ Gauss we find $\omega = 0.025$ eV, which is hardly in the x-ray range. Furthermore, the total energy radiated in one revolution is

$$\frac{\Delta E}{E} = \frac{4\pi}{3}\alpha\gamma^2 \frac{B}{B_{\rm cr}}.$$

For a 23° bend and the above parameters for E and B, we have $\Delta E = 0.0025$ eV, or 0.1 radiated photon per electron. Clearly there can be no significant tail into the keV region.

Concerning scattering off residual gas, suppose we have as much as 10-m path in a vacuum of 10^{-5} torr. Assuming the residual gas to be air, the radiation length at this pressure is then 2×10^{10} m. For 10^5 electrons of 25-MeV energy traversing 10

m of this gas, the total radiated energy is about 5 keV. Hence we might expect one x-ray per pulse. A vacuum of 10^{-6} torr would render the residual gas background completely negligible.

3-6. Data Collection.

Both the readout of the CCD array of the electron spectrometer, and thermal limitations of the final laser amplifier will likely limit the repetition rate of the experiment to less than 10 pulses per second. For the purpose of rate estimates we assume only one pulse per second.

The expected rate of x-ray production per electron is presented in Figure 14, for laser operation at design intensity. As noted in section 3-1, up to 10^5 electrons per pulse can be provided by the Accelerator Test Facility. With a total scattering probablility of 0.4 per electron, some 4×10^4 x-rays will be produced each pulse. These are largely due to first harmonic scattering, which populates the 0–10 keV region of the x-ray spectrum. In a 1% energy bin (100 ev) we then expect about 400 x-rays per pulse. Statistical accuracy of 2% would be obtained with only 10 pulses.

The graphite-mosaic-crystal spectrometer will collect x-rays only within about 10 mrad of the electron-beam direction. Refering to Figure 18, we see that we will be able to explore readily only the upper 20% of the energy range of each harmonic. That is, some 20 spectrometer settings of 1% bandwidth would constitute a data run at each harmonic.

According to Figure 14, the data rate at the third harmonic will be about 1/1000 that at the first harmonic. Good statistical accuracy could then be obtained in one hour of running, 3600 pulses. A scan of 20 spectrometer settings would take one day.

In section 3-4 we mentioned the need to calibrate the x-ray spectrometer on the ordinary Thomson-scattering spectrum obtained with a low-intensity laser beam. To avoid any nonlinear mass-shift effect on the spectrum to the 1% level, the laser field-intensity parameter η^2 should be less than 0.001. (Recall from section 2-3 that the position of the 'Compton edge' of the energy spectrum is multiplied by $1/(1+\eta^2)$ in a strong field.) As the laser photon flux is also proportional to η^2, the scattering rate would then be 160 times smaller than that at the nominal operating condition of $\eta = 0.4$. Thus in the calibration run, which can only explore the first harmonic scattering, there will be about 3 x-rays per pulse in a 1% energy bin. Calibration data should be collected for about one hour at each spectrometer setting, for a total

of one day's running. To calibrate the spectrometer at energies above 10 keV, the electron beam energy will be raised. For example, 20-keV x-rays will be studied with 35-MeV electrons, and 30-keV x-rays with 43-MeV electrons, noting that the scattered x-ray energy varies as the square of the electron-beam energy. In each case the calibration should take about one day.

Thus once the apparatus is fully working, the entire data collection could be performed in about 24 hours, with final calibration occupying several days. We feel this is consistent with the nature of a demonstration experiment, in which the greatest amount of time will be spent in perfecting the novel technologies required.

3-7. The Possiblity of Coherent Scattering.

In this section we examine the suggestion that it might be possible to obtain an enhancement of the x-ray production rate by the coherent interaction of a bunched electron beam with the laser beam.[116,117] We find it unlikely that any coherence effect for x-rays can be arranged in the proposed apparatus. We do not consider the possibility of stimulated Compton scattering,[118] which would require as the seed x-ray intensities (due to unstimulated Compton scattering) far beyond those achievable.

Our analysis is based on rather simple arguments. Following Csonka[116], we first consider the case of coherent effects involving only a single bunch of electrons. Then phase differences between radiation from different electrons in the bunch will average to zero unless the bunch size is much less than a wavelength of the light emitted. This test is to be applied not in the laboratory frame, but in the rest frame of the electron bunch. In the case of a 25-MeV electron beam, the boost to the electrons' rest frame is $\gamma = 50$. In this frame the frequency of the laser beam, which meets the electron beam head-on, is 2γ times the lab frequency, and hence the wavelength is $1/2\gamma$ smaller. With a laser of laboratory wavelength 1 μm, the electron bunch length must be less than 0.01 μm in the electrons' rest frame. However, the laboratory length of the electron bunch is $1/\gamma$ times that in the rest frame, due to the Lorentz contraction. Hence the laboratory bunch length must be less than 0.0002 μm. If the laser light has a 10-μm wavlength, the electron bunch must be shorter than 0.002 μm for coherent scattering.

Conceivably a modulation could be induced on the electron beam such that the bunch length is only 1% of the wavelength of the modulation. Even for the case of a 10-μm laser, the modulation length would need to be less than 0.2 μm. Such a modulation could only be caused by an electromagnetic wave of that wavelength,

which is in the ultraviolet. Hence laser technology is unsuitable to provide the needed bunching. One might imagine the use of a beam from a free-electron laser, but this is a very problematic scenario.

De Martini[117] has considered the case of coherence between bunches, rather than within a single bunch, of an electron beam in head-on collision with a laser beam. In this view coherence is possible when the backscattered light has a wavelength which is a submultiple of the bunch spacing, evaluated in the electrons' rest frame of course. More precisely, we need $2\lambda_b^\star = n\lambda^\star$, thinking of the scattering in analogy with Bragg's law, where $\lambda_b^\star$ is the spacing of the electron bunches and $\lambda^\star$ is the wavelength of the laser light in the rest frame. Now such a scattering will be probable only if the electron density distribution has a significant component at the n^{th} harmonic of the bunch spacing. In turn this requires that the bunch length be less than $1/n$ of the bunch spacing. Altogether we infer that the length of an individual bunch must be less than a wavelength of the laser light in the electrons' rest frame, exactly as argued above.

We conclude that there is no simple technology to induce the very fine bunching of the electron beam needed to produce coherent scattering off the laser beam. On the other hand, the incoherent scattering rate achievable with the proposed laser system is very high, and likely is the simplest way to obtain large x-ray fluxes on a picosecond time scale.

4. The Proposed Laser System.

4-1. Overview.

The proposed laser system for the 25-MeV experiment at BNL is an upgrade of the front-end of the laser system being constructed at Los Alamos for the Accelerator Test Facility. The proposed laser could also serve as the front end in the higher performance system needed for the 50-GeV experiments.

The laser system for the 25-MeV experiment will produce a few pulses per second of 0.1-joule energy and 2-picoseconds length at 1.05-μm wavelength. When focused in an $f3$ mirror a peak intensity of 10^{18} watts/cm^2 can be obtained. The laser system is based on a design of the Mourou group at the Laboratory for Laser Energetics at the U. of Rochester.[119,120] The oscillator will be a Quantronix Model 416, or Spectra Physics Series 3000, mode-locked laser with a Nd:YLF rod, which produces 40-ps-wide pulses. After transmission through a long optical fiber the pulse width is stretched to 300 ps, and a frequency 'chirp' imposed by nonlinear interaction in the fiber. A few pulses per second are injected into a Nd:phosphate-glass amplifier, which could be constructed by Quantel Corp. The amplified output pulse is then compressed with a grating pair to 1-ps width. Figures 19 and 20, from ref. 120, sketch the arrangement of this system. The mode-locked laser will operate at 79.33 MHz, synchronized with the sixth subharmonic of the klystron-driver frequency. A small fraction of the final pulse will be sent to the photocathode of the linac gun, and the remainder brought into collision with the linac beam. The upgrade to the ATF front-end laser will cost about \$150K, and take one year to implement.

For the second-round experiments it is necessary to have a laser system which can produces intensities in excess of 10^{19} Watts/cm^2. It is conjectured that the Nd:glass amplifier scheme sketched above can be scaled upwards to produce pulses of greater than 100 Joules, with duration 1 ps or less.[119,120] If this is indeed proven true we would use such an upgraded system. However, an alternate technology has already been demonstrated which is adequate for our purposes. For this the laser system of the 25-MeV experiment (or a copy) serves as pump for a dye-excimer laser system which will produce a few pulses per second each of 0.25-joule energy and of 0.25-picoseconds length. The wavelength is 308 nm, so that when focused in an $f6$ lens, a peak intensity of 10^{20} watts/cm^2 can be achieved. This will likely be the most intense laser beam built to date (although certain existing lasers can in principle be focused to a similar intensity). The estimated cost for the second-phase

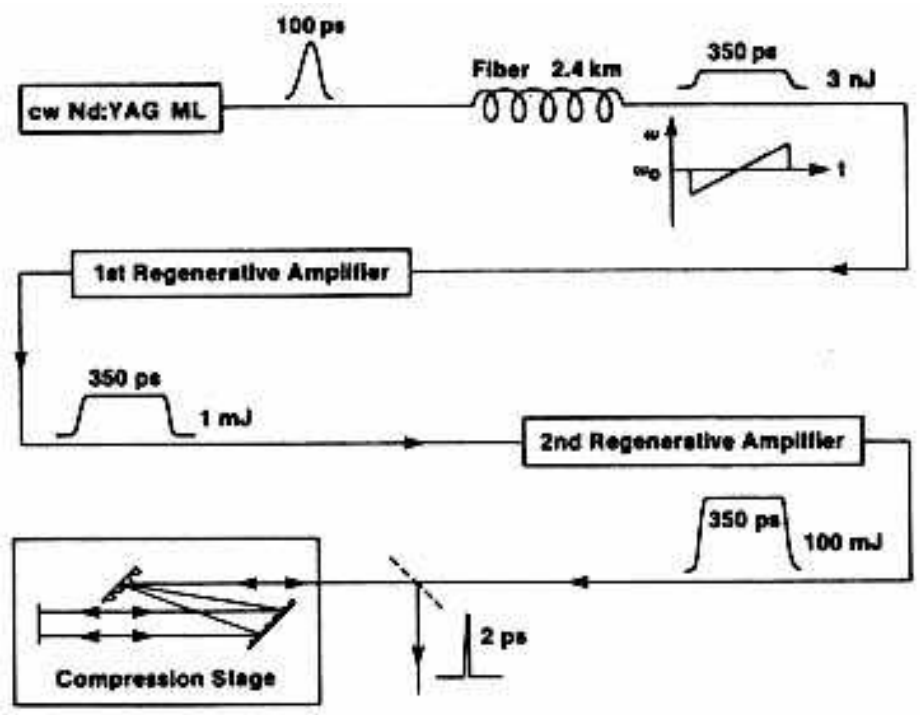

Figure 19. Block diagram of the 1.05-μm wavelength amplication and compression system.[120]

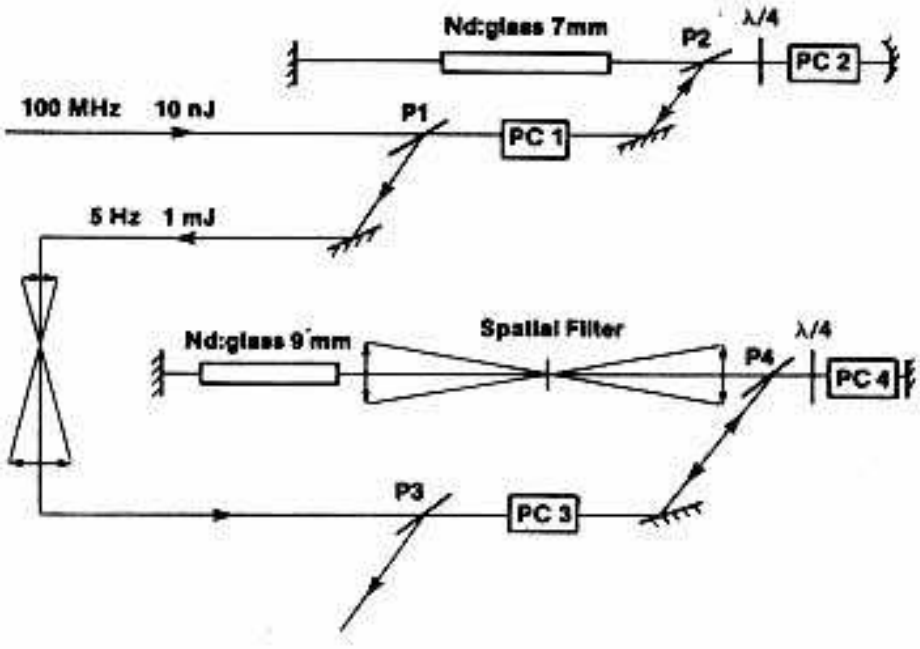

Figure 20. Details of the Nd:glass amplifier.[120]

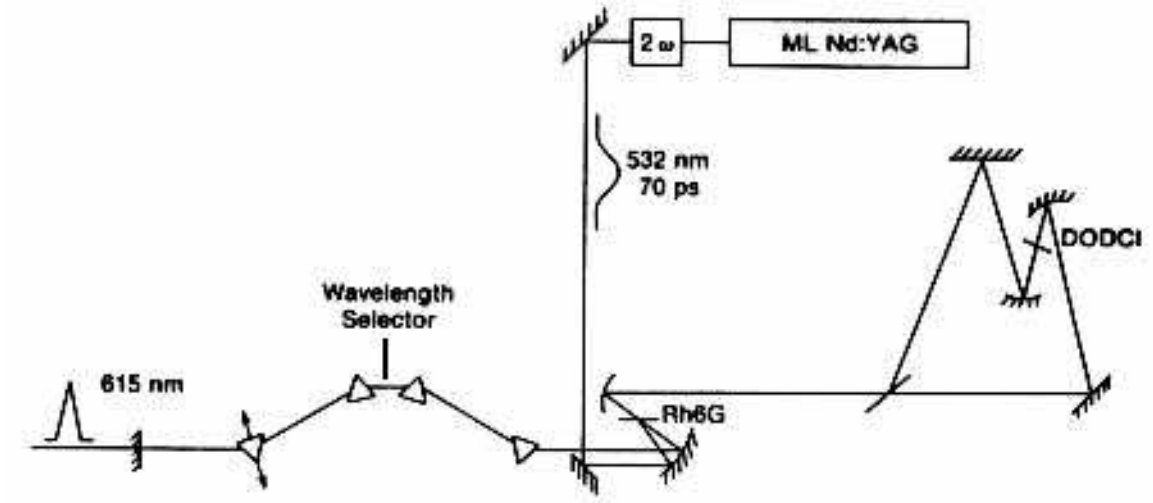

Figure 21. Schematic diagram of the antiresonant-ring dye laser.[122] The saturable absorber (DODCI) is positioned precisely opposite the 50% splitter in the antiresonant ring, allowing colliding-pulse mode locking to occur. The dye laser is synchronously pumped by a frequency-doubled cw mode-locked Nd:YAG (or Nd:YLF) laser.

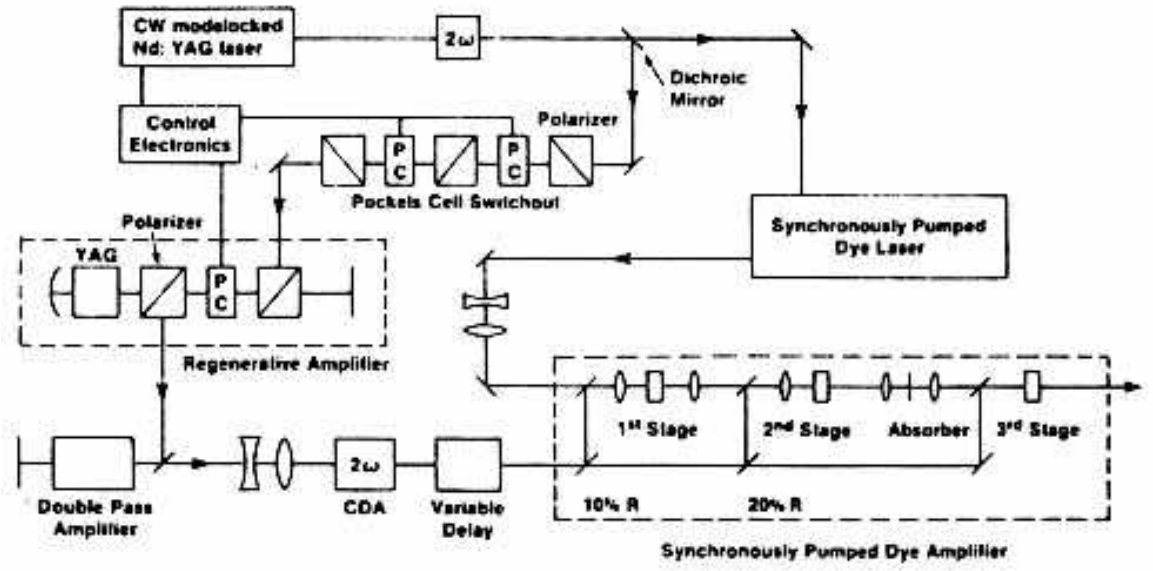

Figure 22. An optically synchronized amplifier for femtosecond pulses.[123]

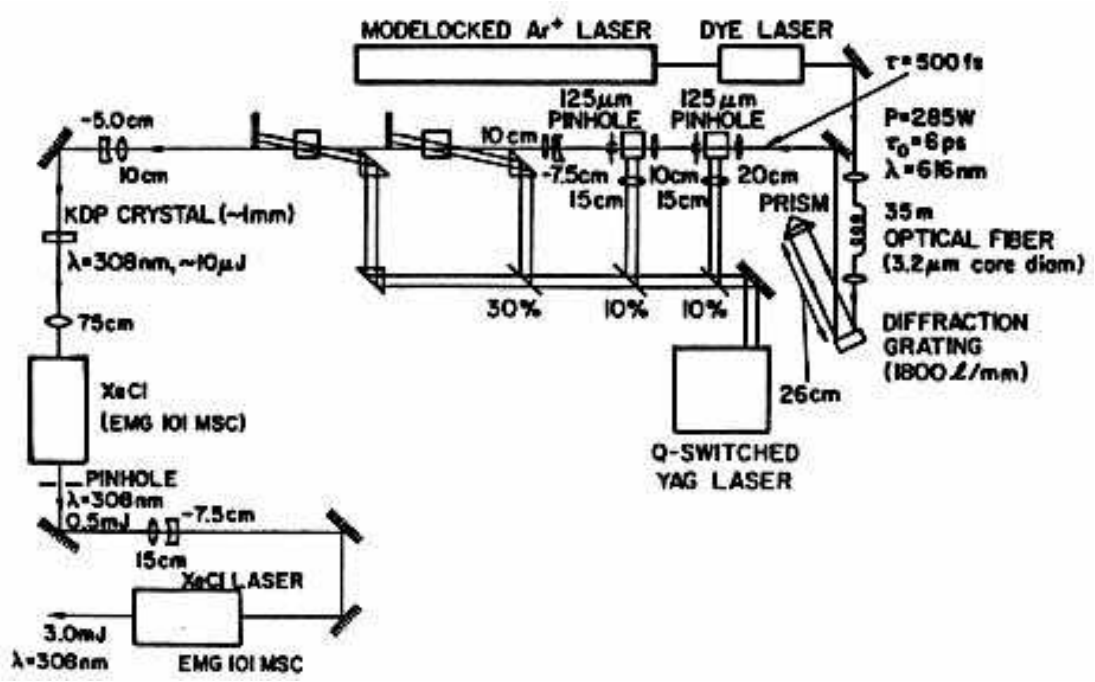

Figure 23. Amplification of 308-nm pulses in a series of XeCl excimer cavities.[124] The 308-nm pulses derive from the frequency-doubled output of a dye-laser system operating at 616-nm.

laser system is an additional $300K.

The laser oscillator is a synchronously-pumped colliding-pulse mode-locked laser[121] operating at 616 nm. A portion of the output of the 1.05-μm mode-locked laser will be frequency-doubled to serve as the pump. The output pulses of 616-nm light will be about 0.1-ps long, and will contain about 0.1 nJoule. Figure 21 sketches the very elegant configuration of such an oscillator.[122] The 616-nm pulses are amplified to about 10 mJ in a 5-stage Nd:YLF-pumped dye-amplifier chain. (The frequency-doubled output of the Quantel amplifier serves as the pump.) Figure 22 sketches a possible layout for the synchronously-pumped amplifier.[123] The amplified 616-nm pulses are then frequency-doubled to 308 nm, and sent through two stages of XeCl excimer amplifiers. Figure 23 sketches such an excimer-amplifier system (driven by a lower performance dye laser).[124] In a double-pass configuration of the final amplifier (such as Helionetics HLX-101) the pulse energy should reach 0.25 joule. The gain-bandwidth of XeCl amplifiers will limit the pulse width to be greater than 150-200 femtoseconds.

All features of this laser system have been demonstrated by members of the laser-physics community, with the important exception of the diffraction-limited character of the final pulse. It is estimated that the construction of such a system

will require 2-3 man-years of very skilled labor in addition to utilizing the excellent resources of commercial laser firms.

4-2. Laser-Linac Synchronization.

Successful running of the experiment will require synchronization of the 2-ps laser pulse with the 2-ps electron bunch to accuracy of about 1 ps. A similar specification holds for the operation of the Accelerator Test Facility for its other purposes as well. As the synchronization is a vital issue we describe how it can be accomplished in some detail, particularly as previous discussions[4] have been very brief.

A block diagram of the synchronization scheme is given in Figure 24. Both the laser and the linac derive their basic timing signals from a crystal reference oscillator, running at 39.666 MHz.† The reference oscillator should have a low aging rate and very low phase noise, such as obtainable with the double-ovenized crystal Model CO-246-A210-VXL2 manufactured by Vectron Laboratories. The 39.666 MHz signal is amplified to drive the acouso-optic mode locker of the laser, which emits a pulse train of frequency twice that applied to the mode locker, namely 79.333 MHz. The 39.666 MHz signal is also frequency-multiplied by 72 to yield the 2856 MHz reference for the klystron. A fast trigger selects a few pulses per second for which the laser pulse is amplified and compressed, and for which the klystron modulator is activated.

It is believed[125] that the timing of the electron bunch as it emerges from the linac will be accurate to 1–2 ps compared to the timing of the reference oscillator, provided that latter has 1-ps timing stability during the 2-μs rf filling time of the linac structure. On the other hand, mode-locked lasers without special synchronization exhibit 5–10-ps timing fluctuations relative to the reference oscillator.[126,127] Hence an extra effort must be made to stabilize the mode locking of the laser.

A simple scheme for stabilizations has been demonstrated by Cotter[126] for a Quantronix laser. This is also sketched in Figure 24. A portion of the 79.333 MHz pulsed output of the laser is converted to electrical pulses in a photodiode, which are then compared with a frequency-doubled signal from the reference oscillator in a phase detector. The latter is a double-balanced mixer, sketched in Figure

† The reference frequency could be any subharmonic of the 2856-MHz klystron frequency that is convenient for the laser operation. The choice of 39.666 MHz is especially favorable if the system were desired to operate at SLAC.

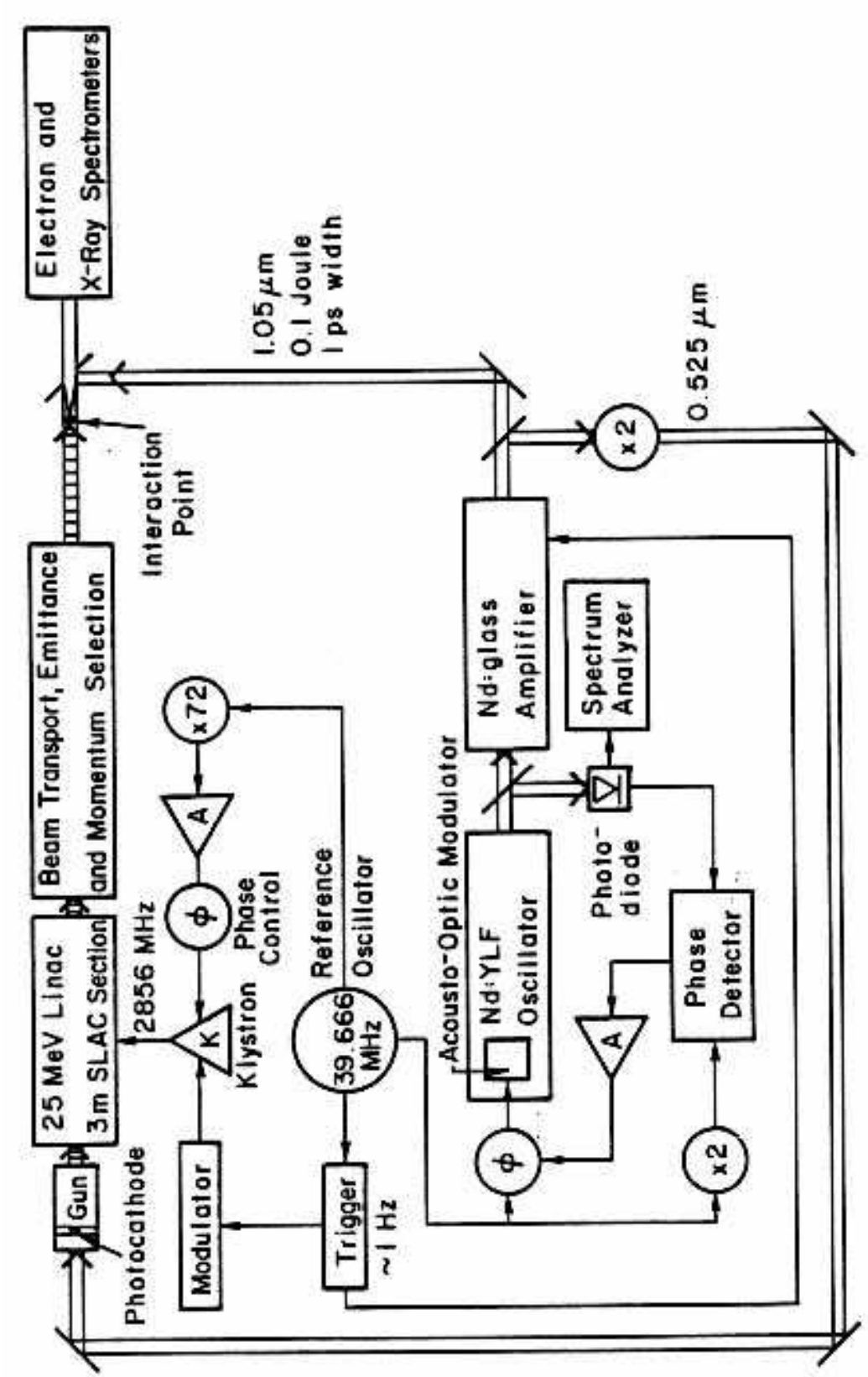

Figure 24. Block diagram of the laser-linac synchronization scheme.

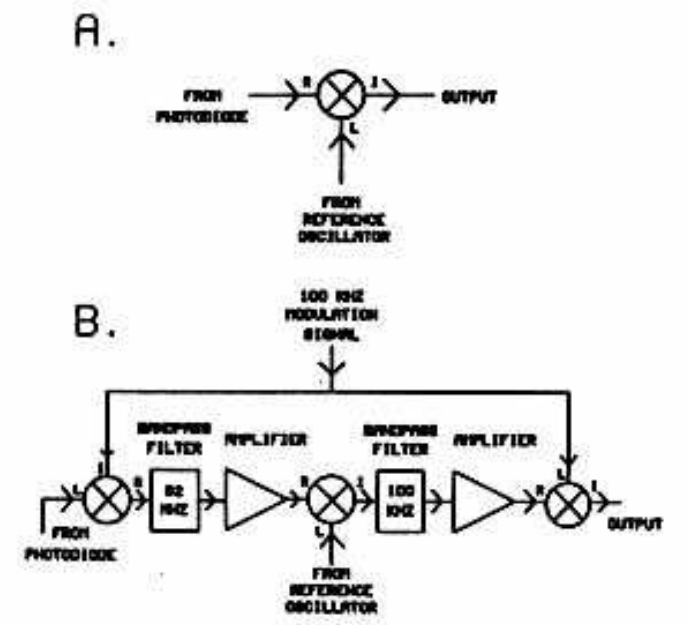

Figure 25. **a.** The double balanced mixer phase detector as used by Cotter.[126]. **b.** The phase detector of Rodwell *et al.*[127] Note the use of the first balanced mixer as a phase shifter.

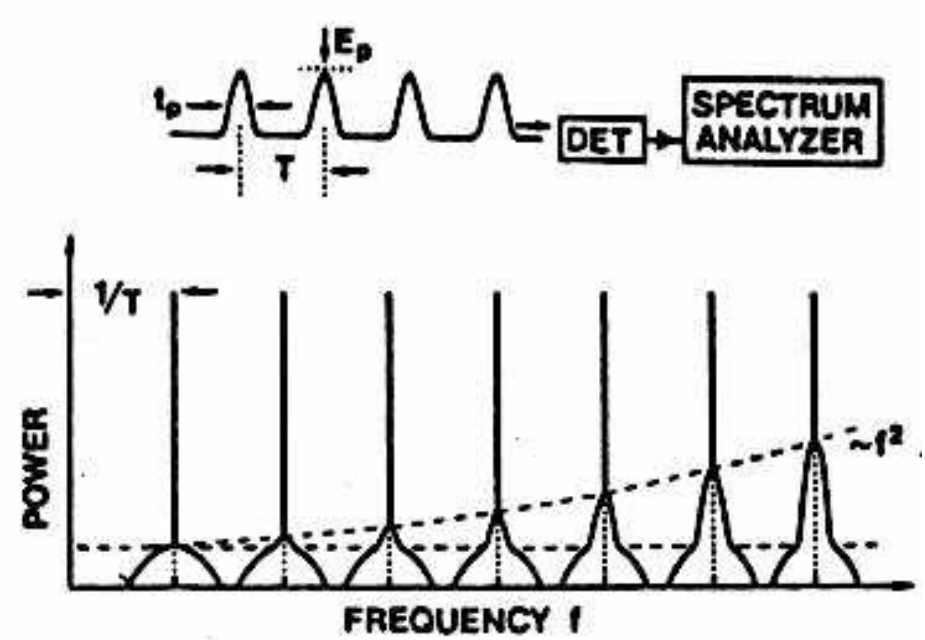

Figure 26. Sketch of the spectrum of the pulse train of a mode-locked laser, showing the sidebands due to amplitude modulation whose intensity is independent of the harmonic number, and the sidebands due to phase modulation whose intensity rises as the square of the harmonic number. After Von der Linde.[128]

25a. The phase error signal is amplified and fed to the voltage-controlled phase shifter which drives the mode locker of the laser. The phase error signal from a typical balanced mixer is about 2 mrad per mV, while a 1-ps shift at 80 MHz corresponds to a phase shift of only 0.5 mrad. At this small signal level effects of amplitude modulation rather than phase modulation may be noticeable in the mixer. The spurious effects of amplitude modulation may be suppressed by the improved phase detector sketched in Figure 25b, as implemented by Rodwell *et al.*[127] Should it prove necessary to provide amplitude stabilization as well as phase stabilization of the Nd laser, we could use a device such as the Cambridge Research and Instrumentation LS-200, in which an electro-optic modulator is controlled by a feedback loop to divert excess amplitude fluctuations of a polarized beam into the other polarization.

Detailed diagnostics of the phase and amplitude modulations can be provided following a technique of Von der Linde.[128] In this the output of the monitor photodiode (Figure 24) is analyzed on a precision spectrum analyzer such as HP 8568B which has a very stable reference oscillator. As sketched in Figure 26 the most prominent feature of the spectrum is the series of near delta function peaks at the harmonics of the laser repetition frequency. Each harmonic peak is surrounded by sidebands at a much lower power level. The effect of amplitude modulation is to produce sidebands whose intensity is independent of the harmonic number n, while the intensity of the phase modulation sidebands rises as n^2. Thus at, say, the 20^{th} harmonic the contribution due to amplitude modulation is negligible compared to that from phase modulations, while the former can be isolated by studying the sidebands at the fundamental. The total power in the phase-modulation sidebands is proportional to the mean-square phase error, so the timing jitter Δt can be found by

$$\left(\frac{n\Delta t}{T}\right)^2 = \frac{1}{P_n}\int_{-\infty}^{\infty} P_{\rm side}(\omega)d\omega,$$

where P_n is the power in the n^{th} harmonic and $P_{\rm side}$ is that in its nearby sidebands. Using this method Rodwell *et al.*[127] verify that a mode-locked Nd:YAG laser may be synchronized to a reference oscillator to 1 ps, as inferred by Cotter[126] directly from the phase-error output of a balanced mixer.

The ultimate test of laser-linac synchronization will of course be that the electron bunch actually collides with the laser beam. The simplest evidence for this will be detection of the backscattered x-rays, as proposed in the present experiment. That is, the essential features of this experiment will be needed as a diagnostic of

e-laser collisions for whatever purpose.

It may be useful to have an additional check of the synchronization which compares the 2856-MHz klystron rf signal with the laser pulses, either before or after amplification of the latter. This could be implemented without actual acceleration of electrons, but otherwise would test all features of the system. A possible device is a GaAs crystal in which 2856-MHz standing sound waves are generated via a transducer (such as made by Brimrose Co.), in a manner similar to the operation of the acousto-optic mode locker of the Nd laser. The intensity of the laser pulse which scatters off the Bragg planes formed by the standing waves is then proportional to $\sin^2\phi$ where ϕ is the phase difference between the laser pulse and the 2856-MHz rf wave.

4-3. Laser Diagnostics.

In addition to the diagnostics of the laser-linac synchronization just described it will be necessary to have several other measures of the laser performance.

As a zeroeth order check of the pulse width of the Nd:YLF oscillator, the output of the monitor photodiode (Figure 24) can be viewed on a sampling oscilloscope, such a Tektronix mainframe 7704 with 7S11 and 7T11 plugins and an S-4 sampling head. The rise time of the best sampling scope is only 25 ps, so the details of the optimized pulse shape cannot be studied this way, but this is the most direct method to diagnose serious departures from nominal performance. Full information on the 40-ps pulse width of the laser oscillator could be provided by a spectrum analyzer of bandwidth greater than 25 GHz, such as the HP 8566B. However, it is more effective to use the cheaper and lower bandwidth HP 8568B analyzer solely as a diagnostic of the pulse synchronization, and study the spectral content of the pulse on a scanning Fabry-Perot interferometer, such as the Burleigh RC-110. An independent measure of the oscillator-pulse width will be provided by an autocorrelator, such as the Femtochrome FR-103 or Inrad 514, based on second harmonic generation in a KDP crystal. These devices produce a complete autocorrelation trace at about 30 Hz.

Additional diagnostics are required for the output of the Nd:glass amplifier, which operates at only a few Hz. Hence devices capable of measurements on a single shot are needed here. The 1-ps pulse shape can be monitored in a novel variation of the autocorrelation technique recently demonstrated by Saltiel *et al.*[129] In this a point image of the amplified laser pulse is transformed into two line images, and a variable delay imposed on one of them. When the two line images are superimposed at the face of a KDP crystal the complete autocorrelation function can be mapped

with a single pulse. The total energy in each pulse will be monitored with a power meter such as Gentec ED500. The profile of each pulse will be recorded by a CCD array, such as Panasonic WVCD50 with a Microdisk Co. Frame Grabber readout.

The cost of the eight diagnostic instruments identified in this and the previous section is somewhat over $100k.

References

1. K.T. McDonald, 'Fundamental Physics During Violent Accelerations,' in 'Laser Acceleration of Particles,' AIP Conference Proceedings No. 130, ed. by C. Joshi and T. Katsouleas (New York, 1985), p. 23.
2. See for example, 'Puzzling Positron Peaks Appear in Heavy-Ion Collisions at GSI,' Physics Today **38**, No. 11, p. 17 (Nov. 1985).
3. W. Greiner *et al.*, *Quantum Electrodynamics of Strong Fields*, (Springer-Verlag, 1985).
4. R.B. Palmer *et al.*, 'Laser Accelerator Test Beam,' (August 27, 1985), unpublished.
5. J.F. Holzrichter *et al.*, 'Research with High-Power Short-Wavelength Lasers,' Science **229**, 1045 (1985).
6. P. Eisenberger, 'A 6-GeV Storage Ring: An Advanced Photon Research Facility,' Science **231**, 687 (1986).
7. See ref. 4, and R.B. Palmer, 'A Laser-Driven Grating Linac,' Part. Accel. **11**, 81 (1980).
8. S.J. Brodsky *et al.*, 'Laser-Induced Axion Photoproduction,' Phys. Rev. Lett. **56**, 1763 (1986).
9. See for example, P.A. Sturrock, 'A Model of Pulsars,' Astro. J. **164**, 529 (1971).
10. J. Arons and E.T. Scharlemann, 'Pair Formation Above Pulsar Polar Caps,' Astro. J. **231**, 854 (1979).
11. H. Herold *et al.*, 'Can γ Quanta Really Be Captured by Pulsar Magnetic Fields,' Phys. Rev. Lett. **54**, 1452 (1985).
12. M. Ruderman, 'High Energy Radiation from Neutron Stars,' SLAC-PUB-3658 (April 1985).
13. T. Erber, 'The Index of Refraction of a Magnetic Field,' in *High Magnetic Fields*, ed. by H. Kolm *et al.* (Technology Press, Cambridge, MA, 1962), p. 706.
14. K.O. Mikaelian, 'Photoproduction of Charged Intermediate Vector Bosons,' Phys. Rev. D **17**, 750 (1978).
15. K.O. Mikaelian, 'Zeroes in $\gamma + e \to W + \nu$,' Phys. Rev. D **30**, 1115 (1984).
16. I.F. Ginzburg *et al.*, '$W^{\pm}$ Boson Production at the e^+e^-, γe and $\gamma\gamma$ Colliding Beams,' Nuc. Phys. **B228**, 285 (1983).
17. A. Salam and J. Strathdee, 'Transition to CP Conservation and Zero Cabibbo Angle in Strong Magnetic Fields,' Nature **252**, 569 (1974).

18. A. Salam and J. Strathdee, 'Transition Electromagnetic Fields in Particle Physics,' Nuc. Phys. **B90**, 203 (1975).
19. T.W.B. Kibble *et al.*, 'Intensity-Dependent Mass Shift and Symmetry Breaking,' Nuc. Phys. **B96**, 255 (1975).
20. A.I. Nikishov and V.I. Ritus, 'Quantum Processes in the Field of a Plane Electromagnetic Wave and in a Constant Field. II,' Sov. Phys. JETP **19**, 1191 (1964).
21. N.B. Narozhny *et al.*, 'Quantum Processes in the Field of a Circularly Polarized Electromagnetic Wave,' Sov. Phys. JETP **20**, 622 (1965).
22. W. Becker *et al.*, 'Laser Enhancement of Nuclear β Decay,' Phys. Rev. Lett. **47**, 1262 (1981).
23. L.D. Landau and E.M. Lifshitz, *The Classical Theory of Fields*, 4^{th} ed. (Pergamon Press, 1975), prob. 2, §47, p. 112, and probs. 2,3, §48, p. 118; this problem appeared in §46 of the 1941 Russian edition.
24. D.M. Volkov, 'Über eine Klasse von Lösungen der Diracschen Gleichung,' Z. f. Phys. **94**, 250 (1935).
25. The mass shift was first noted in N.D. Sengupta, 'On the Scattering of Electromagnetic Waves by a Free Electron,' Bull. Math. Soc. (Calcutta) **44**, 175 (1952).
26. See also V.B. Berestetskii *et al.*, *Quantum Electrodynamics*, (Pergamon Press, 1982), §40, p. 148.
27. L.S. Brown and T.W.B. Kibble, 'Interaction of Intense Laser Beams with Electrons,' Phys. Rev. **133**, A705 (1964).
28. See for example, A.L. Robinson, 'Atoms in Strong Laser Fields Obey the Rules,' Science **232**, 1193 (1986).
29. T.W.B. Kibble, 'Refraction of Electron Beams by Intense Electromagnetic Waves,' Phys. Rev. Lett. **16**, 1054 (1966);
30. T.W.B. Kibble, 'Mutual Refraction of Electrons and Photons,' Phys. Rev. **150**, 1060 (1966).
31. J.J. Thomson, 'The Magnetic Properties of Systems of Corpuscles Describing Circular Orbits,' Phil. Mag. **6**, 673 (1903).
32. G.A. Schott, *Electromagnetic Radiation*, (Cambridge University Press, 1912).
33. J.H. Eberly and A. Sleeper, 'Trajectory and Mass Shift of a Classical Electron in a Radiation Pulse,' Phys. Rev. **176**, 1570 (1968).
34. For a review with extensive references, see J.H. Eberly, 'Interaction of Very Intense Light with Free Electrons,' Prog. in Opt. **VII**, 359 (1969).

35. N.H. Burnett *et al.*, 'Harmonic Generation in CO_2 Laser Target Interaction,' Appl. Phys. Lett. **31**, 172 (1977)
36. E.A. McLean *et al.*, Appl. Phys. Lett. **31**, 825 (1977).
37. R.L. Carman *et al.*, 'Observation of Harmonics in the Visible and Ultraviolet Created in CO_2-Laser-Produced Plasmas,' Phys. Rev. A **24**, 2649 (1981).
38. T.J. Englert and E.A. Rinehart, 'Second-Harmonic Photons from the Interaction of Free Electrons with Intense Laser Radiation,' Phys. Rev. A **28**, 1539 (1983).
39. H. Motz, 'Applications of the Radiation from Fast Electron Beams,' J. Appl. Phys. **22**, 527 (1951).
40. M. Billardon *et al.*, Recent Results of the ACO Storage Ring Free Electron Laser Experiment,' J. de Phys., Colloq. **44**, C1 (1983).
41. B. Girard *et al.*, 'Optical Frequency Multiplication by an Optical Klystron,' Phys. Rev. Lett. **53**, 2405 (1984).
42. A.I. Nikishov and V.I. Ritus, 'Quantum Processes in the Field of a Plane electromagnetic Wave and in a Constant Field. I,' Sov. Phys. JETP **19**, 529 (1964).
43. I.I. Gol'dman, 'Intensity Effects in Compton Scattering,' Sov. Phys. JETP **19**, 954 (1964): and also Phys. Lett. **8**, 103 (1964).
44. A.I. Nikishov and V.I.Ritus, 'Nonlinear Effects in Compton Scattering and Pair Production Owing to Absorption of Several Photons,' Sov. Phys. JETP **20**, 757 (1965).
45. See also §101 of ref. 26.
46. E.J. Williams, 'Correlation of Certain Collision Problems with Radiation Theory,' Kgl. Dansk Vid. Selsk. Mat.-Fys. Medd. **13**, No. 4 (1935).
47. J. Ballam *et al.*, 'Proposal to Move the SLAC Hybrid Facility into a 20 GeV Backscattered Laser Beam,' SLAC Proposal BC-72 (1978).
48. J.E. Brau *et al.*, 'The Lead Glass Columns: A Large Shower Detector at the SLAC Hybrid Facility,' Nuc. Instr. Meth. **196**, 403 (1982).
49. J.C. Kent, 'Charmed-Particle Photoproduction Cross Section at 20 GeV/c,' Ph.D. Thesis, U.C. Berkeley (1983), Report No. UCPPG83-05-20.
50. O. Halpern, 'Scattering Processes Produced by Electrons in Negative Energy States,' Phys. Rev. **44**, 855 (1933).
51. G. Breit and J.A. Wheeler, 'Collision of Two Light Quanta,' Phys. Rev. **46**, 1087 (1934).

52. O. Klein, 'Die Reflexion von Elektronen an einem Potentialsprung nach der relativistischen Dynamik von Dirac,' Zeits. f. Phys. **53**, 157 (1929).
53. F. Sauter, 'Über das Verhalten eines Elektrones im homogenen elektrischen Feld nach der relativistisches Theorie Diracs,' Zeits. f. Phys. **69**, 742 (1931). See also §129, prob. 2 of ref. 26.
54. H.R. Reiss, 'Absorption of Light by Light,' J. Math. Phys. **3**, 59 (1962).
55. A.I. Nikishov and V.I. Ritus, 'Pair Production by a Photon and Photon Emission by an Electron in the Field of an Intense Electromagnetic Wave and in a Constant Field,' Sov. Phys. JETP **25**, 1135 (1967).
56. F.V. Bunkin and I.I. Tugov, 'Possibility of Creating Electron-Positron Pairs in a Vacuum by the Focusing of Laser Radiation,' Sov. Phys. Doklady **14**, 678 (1970).
57. H.R. Reiss, 'Production of Electron Pairs from a Zero-Mass State,' Phys. Rev. Lett. **26**, 1072 (1971).
58. H.R. Reiss, 'Determination of the Intense-Field Mass Shift of the Electron from Vacuum Polarization on the Mass Shell,' Phys. Rev. D **6**, 385 (1972).
59. H. Euler and B. Kockel, 'Über die Streuung von Licht an Licht nach der Diracschen Theorie,' Naturw. **23**, 246 (1935).
60. A. Achieser, 'Über die Streuung von Light an Licht,' Phys. Zeits. d. Sowjetunion **11**, 263 (1937).
61. R. Karplus and M. Neuman, 'The Scattering of Light by Light,' Phys. Rev. **83**, 776 (1951).
62. W. Becker and H. Mitter, 'Vacuum Polarization in Laser Fields,' J. Phys. A **8**, 1638 (1975).
63. B. de Tollis, 'The Scattering of Photons by Photons,' Nuovo Cim. **35**, 1182 (1965).
64. Ian Affleck, private communication.
65. S.L. Adler, 'Photon Splitting and Photon Dispersion in a Strong Magnetic Field,' Ann. Phys. **67**, 599 (1971).
66. See also §130 of ref. 26.
67. A.L. Hughes and G.E.M. Jauncey, 'An Attempt to Detect Collisions of Photons,' Phys. Rev. **36**, 773 (1930).
68. S. Vavilov, 'On the Attempt to Detect Collisions of Photons,' Phys. Rev. **36**, 1590 (1930).
69. V.M. Harutyunian *et al.*, 'Scattering of Light by Light,' Phys. Lett. **6**, 175 (1963).

70. G. Rosen and F.C. Whitmore, 'Experiment for Observing Vacuum Scattering of Light by Light,' Phys. Rev. **137**, B1357 (1965).
71. K.O. Mikaelian, 'Detection of Elastic Light-by-Light Scattering at SLAC,' Phys. Lett. **115B**, 267 (1982).
72. G. Jarlskog *et al.*, 'Measurement of Delbrück Scattering and Observation of Photon Splitting at High Energies,' Phys. Rev. D **8**, 3813 (1973).
73. J.S. Toll, 'The Dispersion Relation for Light and Its Application to Problems Involving Electron Pairs,' Ph.D. Dissertation, Princeton University (1952).
74. W.-Y. Tsai and T. Erber, 'Propagation of Photons in Homogeneous Magnetic Fields: Index of Refraction,' Phys. Rev. D **12**, 1132 (1975).
75. E. Brezin and C. Itzykson, 'Polarization Phenomena in Vacuum Nonlinear Electrodynamics,' Phys. Rev. D **3**, 618 (1971).
76. T. Erber, 'Velocity of Light in a Magnetic Field,' Nature **190**, 25 (1961).
77. J.J. Klein and B.P. Nigam, 'Birefringence of the Vacuum,' Phys. Rev. **135**, B1279 (1964).
78. J.J. Klein and B.P. Nigam, 'Dichroism of the Vacuum,' Phys. Rev. **136**, B1540 (1964).
79. M. Lutzky and J.S. Toll, 'Formation of Discontinuities in Classical Nonlinear Electrodynamics,' Phys. Rev. **113**, 1649 (1959).
80. K.D. Bonin *et al.*, 'Observation of Interference between Čerenkov and Synchrotron Radiation,' Phys. Rev. Lett. **57**, 2264 (1986).
81. D.A. Bagdasaryan *et al.*, 'Čerenkov Radiation from a Propagating Nonlinear Polarization Wave,' JETP Lett. **37**, 594 (1983).
82. D.H. Auston *et al.*, 'Čerenkov Radiation from Femtosecond Optical Pulses in Electro-Optic Media,' Phys. Rev. Lett. **53**, 1555 (1984).
83. S.W. Hawking, 'Black Hole Explosions?' Nature **248**, 30 (1974); 'Particle Creation by Black Holes,' Comm. Math.-Phys. **43**, 199 (1975).
84. S.A. Fulling, Ph.D. Dissertation, Princeton University (1972); 'Nonuniqueness of Canonical Field Quantization in Riemannian Space-Time,' Phys. Rev. D **7**, 2850 (1973).
85. P.C.W. Davies, 'Scalar Particle Production in Schwarzschild and Rindler Metrics,' J. Phys. A **8**, 609 (1975).
86. W.G. Unruh, 'Notes on Black Hole Evaporation,' Phys. Rev. D **14**, 870 (1976); 'Particle Detectors and Black Hole Evaporation,' Ann. N.Y. Acad. Sci. **302**, 186 (1977).

87. D.W. Sciama, 'The Thermodynamics of Black Holes,' Ann. N.Y. Acad. Sci. **302**, 161 (1977).
88. D.W. Sciama, P. Candelas and D. Deutsch, 'Quantum Field Theory, Horizons and Thermodynamics,' Adv. in Phys. **30**, 327 (1981).
89. W.D. Birrell and P.C.W. Davies, *Quantum Fields in Curved Spacetime*, (Cambridge University Press, 1982).
90. T.H. Boyer, 'Thermal Effects of Acceleration Through Random Classical Radiation,' Phys. Rev. D **21**, 2137 (1980); 'The Classical Vacuum,' Sci. Am. **253**, No. 2, 70 (August, 1985).
91. J.F. Donoghue and B.R. Holstein, 'Temperature Measured by a Uniformly Accelerated Observer,' Am. J. Phys. **52**, 730 (1984).
92. U.H. Gerlach, 'Emission of Blackbody Radiation from an Accelerated Charge,' University of Ohio preprint (1982), unpublished.
93. N.P. Myhrvold, 'Vistas in Curved Space-Time Quantum Field Theory,' Ph.D. Dissertation, Princeton University (1983).
94. V.I. Ritus, 'The Mass Shift of an Accelerated Charge,' Sov. Phys. JETP **53**, 659 (1981).
95. J.S. Bell and J.M. Leinaas, 'Electrons as Accelerated Thermometers,' Nuc. Phys. **B212**, 131 (1983).
96. A.A. Sokolov and I.M. Ternov, 'On Polarization and Spin Effects in the Theory of Synchrotron Radiation,' Sov. Phys. Doklady **8**, 1203 (1964); see also §90 of ref. 26.
97. A. Salam and J. Strathdee, 'Hadronic Temperature and Black Solitons,' Phys. Lett. **66B**, 143 (1977).
98. S. Barshay and W. Troost, 'A Possible Origin for Temperature in Strong Interactions,' Phys. Lett. **73B**, 437 (1978).
99. A. Hosoya, 'Moving Mirror Effects in Hadronic Reactions,' Prog. Theor. Phys. **61**, 280 (1979).
100. W.A. Bardeen *et al.*, 'Static Quantities in Weinberg's Model of Weak and Electromagnetic Interactions,' Nuc. Phys. **B46**, 319 (1972).
101. O.P. Sushkov *et al.*, 'A Test of the Renomralizable Models of Weak Interactions in e^+e^- Collisions,' Sov. J. Nuc. Phys. **20**, 537 (1975).
102. W. Alles *et al.*, 'W Boson Production in e^+e^- Collisions in the Weinberg-Salam Model,' Nuc. Phys. **B119**, 125 (1977).
103. R.P. Feynman, 'Sapce-Time Approach to Quantum Electrodynamics,' Phys. Rev. **76**, 769 (1949).

104. T.D. Lee and C.N. Yang, 'Theory of Charged Vector Mesons Interacting with the Electromagnetic Field,' Phys. Rev. **128**, 885 (1962).

105. T.D. Lee, 'Application of ξ-Limiting Process to Intermediate Bosons,' Phys. Rev. **128**, 899 (1962).

106. C. Akerlof, 'Using the SLC as a Photon Accelerator,' University of Michigan preprint UM HE 81-59 (1981).

107. É.A. Choban, 'Production of Neutral Vector Mesons and an Intermediate Boson in Colliding Lepton Beams,' Sov. J. Nuc. Phys. **13**, 354 (1971).

108. A.M. Altukhov and I.B. Khriplovich, 'Single Production of W Boson in Colliding Electron Beams,' Sov. J. Nuc. Phys. **13**, 359 (1971).

109. A.M. Altukhov, 'Single Production of W Boson in Colliding Electron-Positron Beams,' Sov. J. Nuc. Phys. **13**, 362 (1971).

110. I.F. Ginzburg *et al.*, 'Colliding γe and $\gamma\gamma$ beams Based on the Single-Pass e^+e^- Colliders (VLEPP Type),' Nuc. Instr. Meth. **205**, 47 (1983).

111. J.E. Spencer and S.J. Brodsky, 'Breeding New Light into Old Machines (and New),' SLAC-PUB-3646 (1985).

112. A. Yariv, *Quantum Electronics*, 2^{nd} ed. (Wiley, 1975).

113. R.H. Miller, presented at the Accelerator Test Facility Group meeting (Brookahven Lab, July 10-11, 1986).

114. C.K. Sinclair and R.H. Miller, 'A High Current, Short Pulse, RF Synchronized Electron Gun for the Stanford Linear Accelerator,' IEEE Trans. Nuc. Sci. **NS-28**, 2649 (1981).

115. R.W. Gould *et al.*, 'Application of the Graphite Monochromator to Light Element X-Ray Spectroscopy,' Appl. Spectr. **22**, 549 (1968); C.J. Sparks, Jr., 'Mosaic Crystals for Obtaining Larger Energy Bands and High Intensities from Synchrotron Radiation Sources,' in *Workshop on X-Ray Instrumentation for Synchrotron Radiation Research*, ed. by H. Winick and G. Brown (SSRL Report 78/04, Stanford, 1978), p. III-35.

116. P.L. Csonka, 'Enhancement of Synchrotron Radiation by Beam Modulation,' Part. Accel. **8**, 225 (1978).

117. F. De Martini, 'An X-Ray Relativistic Free-Electron Frequency Converter,' in *Physics of Quantum Electronics* Vol. VII, Ed. by S.F. Jacobs (Addison-Wesley, 1980), p. 789.

118. R.H. Pantell *et al.*, 'Stimulated Photon-Electron Scattering,' IEEE J. Q.E. **4**, 905 (1968).

119. D. Strickland and G. Mourou, 'Compression of Amplified-Chirped Optical Pulses,' Opt. Comm. **55**, 447 (1985); G. Mourou *et al.*, 'How Pulse Compression Techniques Can Be Applied to High-Energy Laser Amplifiers,' Laser Focus, p. 104 (June, 1986).
120. D. Strickland *et al.*, 'Picosecond Pulse Amplification Using Pulse Compression Techniques,' U. of Rochester preprint (June, 1986), to appear in the Proceedings of the 1986 Conference on Ultrafast Phenomena (Snowmass, 1986).
121. R.L. Fork *et al.*, 'Femtosecond Optical Pulses,' IEEE J. Q.E. **19**, 500 (1983).
122. T. Norris *et al.*, 'Generation of Microjoule, 65-fs Pulses at High Repetition Rate,' Proceedings of the Conference on Lasers and Electro-Optics (Baltimore, 1985), p. 38.
123. T. Sizer II *et al.*, 'Synchronous Amplification of Subpicosecond Pulses,' IEEE J. Q.E. **19**, 506 (1983).
124. J.H. Glownia *et al.*, 'Amplification of 350-fsec Pulses in XeCl Excimer Gain Modules,' Opt. Lett. **11**, 79 (1986).
125. Heinz Schwartz, SLAC RF Group (private communication).
126. D. Cotter, 'Technique for Highly Stable Active Mode-Locking,' in *Ultrafast Phenomena IV*, ed. by (Springer-Verlag, 1984), p. 78; U.K patent application GB2161980A (22 Jan. 1986).
127. M.J.W. Rodwell *et al.*, 'Reduction of Timing Fluctuations in a Mode-Locked Nd:YAG Laser by Electronic Feedback,' Opt. Lett. **11**, 638 (1986).
128. D. Von der Linde, 'Characterization of the Noise in Continuously Operating Mode-Locked Lasers,' Appl. Phys. B **39**, 201 (1986).
129. S.M. Saltiel *et al.*, 'Realization of a Diffraction-Grating Autocorrelator for Single-Shot Measurement of Ultrashort Light Pulses Duration,' Appl. Phys. B **40**, 25 (1986).